SMALL LESION DETECTION WITH RESOLUTION ENHANCEMENT COMPRESSION: A METHOD OF CODED EXCITATION/PULSE COMPRESSION

BY

PAUL MITCHELL LINDEN

THESIS

Submitted in partial fulfillment of the requirements
for the degree of Master of Science in Electrical and Computer Engineering
in the Graduate College of the
University of Illinois at Urbana-Champaign, 2010

Urbana, Illinois

Adviser:

Assistant Professor Michael L. Oelze

Abstract

A novel coded excitation method, resolution enhancement compression (REC), increases the axial resolution and the echo signal-to-noise ratio (eSNR) for an ultrasonic imaging system. The REC technique was examined for its ability to improve lesion detectability. In addition to lesion detectability, the REC technique was examined in the context of being peak voltage limited or peak pressure limited. The REC technique was used to double the –3-dB fractional pulse-echo bandwidth of an ultrasonic source in both simulations and experiments. The increase in usable bandwidth increased lesion detectability compared to conventional pulsing (CP) techniques and coded excitation using a linear chirp (LC). Lesion detectibility was quantified through lesion signal-to-noise ratio (lSNR), which is a metric that quantifies the ability of an isolated observer to detect a focal lesion against a background. In simulations, a higher lSNR value was observed using the pressure limited REC technique for lesions ranging in size from 1 mm to 8 mm in diameter. In addition, the eSNR was increased by almost 15 dB. Simulations also demonstrated that the voltage limited and the pressure limited form of REC outperformed the LC with respect to lSNR. To validate simulation results, a hydrogel cone phantom was constructed to provide lesions of different diameters with +6-dB contrast. A transducer was scanned perpendicular to the major axis of the cone at different levels to provide lesions of 3, 5, and 8 mm in diameter. The lSNR was estimated for lesions of different sizes and using the three excitation techniques, i.e., CP, LC, and REC. In experiments the lSNR was observed to be higher using the REC technique than the other pulsing techniques. The lSNR scores for REC were higher by 15%, 45%, and 40% for the 3, 5, and 8-mm as compared to the other two excitation

techniques. The eSNR was increased by 5.7 dB. Therefore, according to the lSNR metric, the improvement in spatial resolution from the REC technique resulted in improved detectability of small lesions.

Acknowledgments

First, the author would like to thank Dr. Michael L. Oelze. In addition, the author would like to thank Dr. Jose Sanchez for his helpful guidance and the technical assistance of Marko Orescanin in the construction of the cone phantom. This work was supported by a grant from the NIH (R21EB006741).

Table of Contents

Chapter 1 Introduction

1.1 Overview

1.1.1 Objective of the Research

Lesion detectability is a function of the contrast between lesion background, the lesion size, the speckle variance, and the spatial resolution of the imaging system. Resolution enhancement compression (REC) is a method of coded excitation that directly improves spatial resolution and echo signal-to-noise ratio (eSNR). The spatial resolution improvement of REC over other excitation methods should also improve small lesion detectability. In the current study, the REC technique will be examined for its ability to improve target detectability, specifically small lesion detectability.

1.1.2 Medical Imaging

Ultrasonic imaging is a powerful diagnostic tool in the medical imaging community. Ultrasonic imaging's strongest arguments are its low cost, safety (non-ionizing radiation), and portability. Numerous medical imaging modalities exist with different strengths and weaknesses with respect to cost, speed, portability, and resolution. Common medical imaging systems include computed tomography (CT), positron-emission tomography (PET), magnetic resonance imaging (MRI), and X-ray. The spatial resolution of X-ray, CT, and MRI are about 1 mm compared with ultrasonic imaging which ranges from 0.3-3 mm depending on frequency, aperture size, and penetration depth [1]. Penetration depth is limited because ultrasonic waves attenuate as they propagate into tissue reducing signal power. However, because of the low cost, safety, portability, and efficacy, ultrasonic imaging is often the preferred imaging modality [1].

Moreover, about 250 million ultrasound exams were performed in 2000 (Figure 1.1). The United States alone spends more than $5 billion a year on ultrasonic imaging equipment [2].

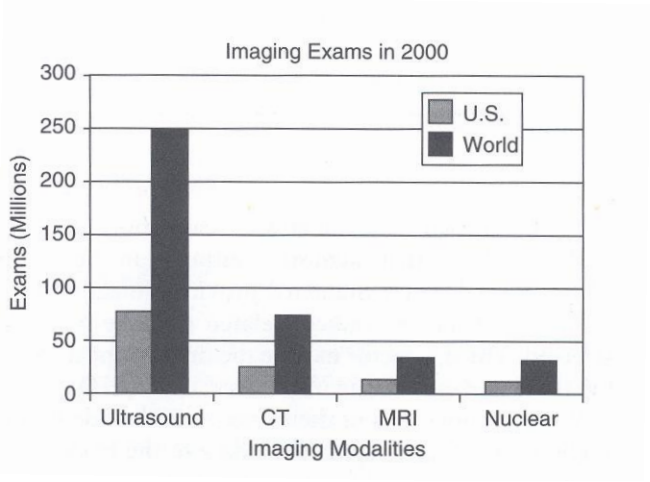

Figure 1.1. Imaging exams in 2000 [1].

The use of ultrasonic waves for imaging of tissue dates back to the 1950s when Wild and Reid proposed echography for the detection of tumors in living humans [3]. Today ultrasonic imaging is used in a variety of settings in the clinic including cardiology; radiology; obstetrics/gynecology; endoscopic; transesophageal and transrectal; surgical, intraoperative, laparoscopic, and neurosurgical; vascular and intravascular [1]. Improvements in diagnostic ultrasonic imaging are expected to come from higher bandwidth transducers, advanced signal-processing and image-reconstruction techniques, and tissue characterization [2], [4]. This work reflects improvements in diagnostic ultrasound through advanced signal-processing and image-reconstruction techniques.

1.2 Literature Review

1.2.1 Ultrasound Image Quality

Improving image quality in a diagnostic ultrasound system is a natural goal. Image quality in ultrasound systems can be characterized by contrast resolution, echo signal-to-noise ratio (eSNR), and spatial resolution. Contrast resolution can be quantified through the contrast-to-noise ratio (CNR). Typically, in ultrasonic imaging, contrast between soft tissues is low compared to other imaging modalities. The reflectivity between tissue interfaces can be as low as 1 part in 10^6 [5]. The impedance mismatch between tissue structures results in the reflection or scattering of ultrasound and it is this reflected ultrasound that is used to produce images. Scattering of sound from objects can be classified into three broad categories: specular, diffractive, and diffusive [1]. Specular refers to scattering from objects much larger than the wavelength; diffractive to objects about the same size as the wavelength; and diffusive refers to scattering from objects much smaller than a wavelength. The speckle in biomedical ultrasound images results from scattering from objects smaller than a wavelength. This scattering is deterministic and cannot be removed by time averaging of the signal. However, information about the sub-wavelength scatterers can be inferred from the backscattered ultrasound [4].

While the speckle in the ultrasound image correlates to information about sub-wavelength scatterers, it can degrade the ability of an ultrasound system to detect low contrast targets or small lesions [5]. Detection of lesions against a background is of prime importance in medical imaging. Examples include the detection of breast masses, focal lesions in the liver, or infracted regions of myocardium [6]. Therefore, much research has been conducted to quantify the detectability of targets using ultrasound

imaging and to improve target detection through various mechanisms, e.g., speckle reduction [7].

A low eSNR can also reduce image quality and mask the ability to perceive contrast in images. Techniques to reduce noise and increase eSNR are important to improving ultrasonic imaging. Low spatial resolution can also lead to reduced image quality and also affect image contrast. Small lesion detection is limited by spatial resolution and image noise [5]. Thus a higher spatial resolution and a higher eSNR are desirable because they can increase the detectability of small lesions.

The spatial resolution in an ultrasound imaging system can be different in the lateral and axial directions. Furthermore, the impulse response is spatially varying over the field. The axial direction is defined as the direction of propagation of the ultrasonic waves, which in the case of a single-element transducer is perpendicular to the major axis of the transducer. The lateral resolution is perpendicular to the propagation direction of the ultrasonic waves. The axial resolution is inversely proportional to the transducer bandwidth and lateral beamwidth is proportional to the aperture size divided by the wavelength [8].

The resolution in the axial direction can be quantified by the ability to resolve two point targets spaced a distance Δz apart in the axial direction. From Figure 1.2, a pulse of longer duration, pulse length >> Δz, and the reflection from target 1 and target 2 will be smeared together rendering them as one large target. However, the pulse of shorter duration, pulse length < Δz, and target 1 and 2 may be resolved as two separate entities. The axial resolution in mm for a Gaussian pulse can be estimated as

$$FWHM_{axial} = \frac{1.37}{\Delta f}, \tag{1.1}$$

where Δf is the -6-dB bandwidth in MHz [8].

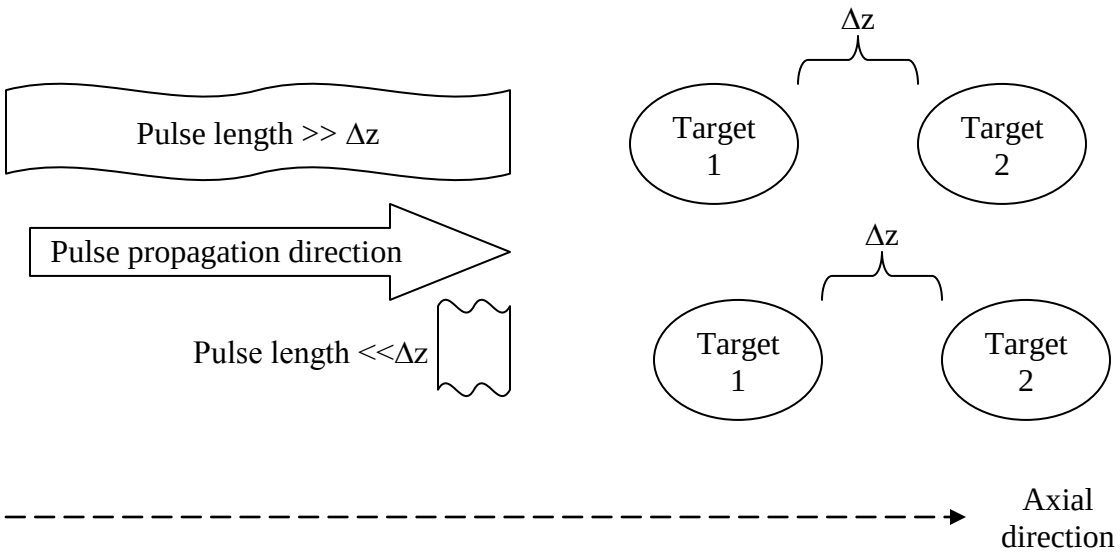

Figure 1.2. Axial resolution and relationship to pulse duration.

There are two simple ways to increase the axial resolution of the ultrasonic imaging system. The first is to keep the same fractional bandwidth but move to a higher frequency. The second method is to keep the same center frequency but increase the fractional bandwidth. However, attenuation in tissue is also a function of frequency and a higher center frequency leads to more severe attenuation, a reduced penetration depth, and a reduction of eSNR. The transducer bandwidth is also a physical property of the transducer which cannot be adjusted. Most transducers, including the ones in this study, are made of piezoelectric material which limits the attainable fractional bandwidth. However, knowing the frequency response of the transducer could allow the excitation signal to be constructed to enhance the response of the transducer and effectively provide

a larger bandwidth. In this thesis, techniques to improve the axial resolution of an imaging system with special coded excitation will be explored in the context of detecting small lesions.

1.2.2 Bioeffects

Adverse biological effects of diagnostic, clinical ultrasound have not yet been reported [9]. However, the Food and Drug Administration (FDA) strictly regulates diagnostic imaging systems and limits exposure. The two major safety concerns are cavitation and heating. The limits are a temporal average intensity, I_{SPTA} (spatial peak time average), of 720 mW/cm^2, and a mechanical index (MI) of 1.9 [9]. The MI measures the potential of ultrasound to inflict damage through mechanical mechanisms and is defined as

$$\mathrm{MI} = \frac{p_{-}(\mathrm{MPa})}{\mathrm{C_{MI}}\sqrt{f(\mathrm{MHz})}}, \tag{1.2}$$

where p_- is the peak rarefactional pressure and C_{MI} is 1.0 MPa/MHz$^{1/2}$ [8]. Common MI values for diagnostic ultrasound are between 0.04 and 1.7 [8]. The limiting factor in commercial systems is the peak transmitted pressure rather than the time-averaged intensity [10]. This limit presents a challenge when imaging patients of a high body mass index (BMI) because peak-pressure is limited and attenuation in tissue degrades signal strength. Thus, numerous authors have proposed transmitting longer waveforms to increase signal strength without increasing peak rarefactional pressure. The goal is to improve the eSNR so that image quality can be improved. However, longer duration signals result in reduced axial resolution in ultrasonic images. Therefore, in conventional

excitation of the ultrasonic sources, there exists a tradeoff between eSNR, signal duration, and axial resolution.

1.2.3 Small Lesion Detection

Much of the framework for quantifying target detectability in biomedical ultrasound was established by Wagner and colleagues [5], [6], [11]. Smith et al. derived contrast/detail curves as a function of contrast, resolution cell volume, and lesion diameter [6]. Interestingly, they found contrast/detail analysis curves for enveloped detected ultrasound images were nearly identical to the square law detector (those used with lasers). Smith et al. noted that these contrast/detail curves suggested that lesion contrast was dependent on lesion diameter at the observer's threshold for lesion detection [6]. Such curves could be used to predict the performance of an imaging system with respect to lesion detection before performing extensive clinical trials in order to yield receiver operator characteristics (ROC) curves. Smith et al. derived an expression based on statistical decision theory to describe the ideal observer [6]. The ideal observer is described as

$$C_\psi D = SNR_T (S_{cx} S_{cz})^{1/2}, \tag{1.3}$$

where C_ψ is the contrast of the lesion (between 0 and 1), D is the diameter of the lesion, and the product of S_{cx} (lateral resolution) and S_{cz} (axial resolution) is the resolution cell volume. SNR_T represents the "threshold" of lesion detectibilty for a fixed level of observer performance. However, once calibrated to an observer, Equation (1.3) predicts the slope of the detection curve (log threshold contrast versus log threshold diameter) is -1. As far as this author has been able to determine, the first mention of lesion signal-to-noise ratio (lSNR) is a 2005 study by Dahl et al. [12], who proposed an lSNR metric,

based on Smith et al. [6], by rearranging Equation (1.3) as

$$SNR_T = \frac{D \cdot CNR}{\sqrt{S_{cx} \cdot S_{cz}}}\sqrt{N}, \tag{1.4}$$

where *N* is the number of independent images used in spatial compounding and CNR is the contrast-to-noise ratio [12].

In addition to the contrast/detail analysis, another metric of paramount importance in any imaging modality for small lesion detection is the eSNR. If eSNR decreases, noise begins to dominate the signal and consequently CNR is reduced as the image is washed out with noise. Conversely, as eSNR is increased a better CNR may be achievable resulting in increased lesion detectibility. Thus, in addition to CNR, a high eSNR is desirable and pre-requisite for small lesion detection. This presents a challenge for ultrasonic imaging since eSNR if of prime importance, yet eSNR degrades as the ultrasonic wave propagates deeper into tissue.

1.2.4 Coded Excitation and Pulse Compression

Scanners that function with a traditional pulse/echo excitation scheme are limited by pulse duration and peak pressure values, which can also limit the eSNR (see section 1.2.2 Bioeffects). The axial resolution of a pulse/echo system is related to the length of the transmitted pulse and peak-pressure is limited by the hardware of the system or by FDA regulations. If the pulse length is appreciably shortened without increasing peak pressure, the axial resolution can improve but the eSNR can decrease, which may result in a reduction in image quality.

One method for boosting the eSNR is through coded excitation techniques.

Coded excitation has been used for decades in radar systems [13]. Radar systems used coded excitation and pulse compression to increase energy per pulse in peak-power limited radar systems [14]. In addition, the longer transmit signal of a coded waveform need not compromise axial resolution if compressed properly [14].

Takeuchi first proposed coded excitation for biomedical ultrasonic imaging in 1979 in a technique called the spread energy method (i.e., FM chirps and phase coding) [15]. However, ultrasonic imaging systems are limited by much smaller bandwidths than radar systems. Therefore, Takeuchi suggested that the only increase in the time-bandwidth product (TBP) comes from increasing the period of the transmitted signal, because the bandwidth of the system was already taken to the limit.

Coded excitation combined with pulse compression is a method that decouples the dependence of axial resolution on pulse length. The axial resolution of a short duration pulse can be approximated as $\tau=1/B$, where B represents the bandwidth of the system and τ is the temporal resolution [16]. The bandwidth of a system is largely limited by the passband nature of the transducer. A typical pulse will have a TBP of approximately unity [17]. Coded excitation includes a broad class of signals with a TBP greater than unity. The TBP quantifies the difference between a single carrier and a coded excitation waveform. Thus a longer signal of desired power and bandwidth can be constructed without a major loss in axial resolution. The longer transmit signal is compressed on receive to restore axial resolution.

Pulse compression can be achieved by inverse filtering, matched filtering, or mismatched filtering, e.g., a Wiener filter. The matched-filter is optimum in the sense that it maximizes the signal-to-noise ratio at the receiver in the presence of additive white

Gaussian noise (AWGN). The matched filter was first described by North in 1942 [18]. The maximum gain from the matched filer is

$$SNR_{Max} = \frac{2\varepsilon_s}{N_0}, \tag{1.5}$$

where ε_s is the energy in the transmit waveform and $N_0/2$ is the power spectral density of the noise [19].

The major drawback to the matched filter is self-noise or sidelobes. One method to suppress sidelobes is by weighting the transmit signal by a window function, a method called mismatch filtering [17]. The correlation method and the matched filter are essentially the same mathematically but implemented differently [14]. A matched filter can be implemented as a filter in the frequency domain or as a correlator in the time-domain at the front end of the receiver. The matched filter is also known as the North filter and the conjugate filter [14]. The matched filter is optimal in the sense that it maximizes the eSNR. The matched filter is described in terms of the transmit waveform $s(t)$. The matched filter to the waveform $s(t)$ is

$$H(f) = GS^*(f)e^{-j2\pi ft}, \tag{1.6}$$

where $S^*(f)$ represents the conjugate of the Fourier transform of $s(t)$ and G is the filter gain. The matched filter could also be realized in its correlation form as

$$R(t) = \int_{-\infty}^{\infty} y(\tau)s(t-\tau)d\tau \tag{1.7}$$

where $y(\tau)$ is the received signal and $s(t)$ is the *a priori* known transmitted wave form. Equation **(**1.7**)** is easily realized in discrete time by replacing the integral with a summation and the continuous-time variables with their discrete-time analogs.

The Wiener filter can be realized in frequency domain as

$$H(f) = \frac{S^*(f)}{S^*(f)S(f) + N_f N_f^*}, \tag{1.8}$$

where N_f is the noise spectrum [17]. The advantage of Wiener filtering is its balance between inverse filtering and matched filtering. In frequency bands where signal strength is low Equation (1.8**)** reduces to a matched filter and when signal strength is high relative to the noise the same equation reduces to an inverse filter. In ultrasonic imaging, operating closer to an inverse filter translates into a preservation of axial resolution which is highly desirable. However, as signal strength declines relative to the noise floor, such as the passband of the transducer, inverse filtering would amplify the noise. However, the Wiener filter will function more as a matched filter in these frequency bands suppressing noise. This has the added effect of minimizing sidelobes, preserving axial resolution, while balancing the eSNR gain.

The inverse filter is an attempt at direct deconvolution. Inverse filtering is implemented by directly dividing the spectrum of the RF data by the spectrum of the known transmitted signal. Theoretically, under extremely low noise situations or with small modifications (to avoid dividing by zero) the inverse filter achieves the best suppression of sidelobes and better spatial resolution than the matched filter. However, noise in the system renders inverse filtering impractical. In addition to dividing by zero, the inverse filter also amplifies noise at high frequencies.

A compromise between the matched filter and the inverse filter is a mismatched filter. In this work the mismatched filter is given by the Wiener filter. The Wiener filter minimizes the mean square error between the signal and the noise in different frequency bands. The Wiener filter allows the user to adjust between noise amplification, sidelobe levels, and spatial resolution.

The increase in eSNR in the correlator or matched filter system is equal to the TBP [17]. Radar systems which operate in the GHz often use TBP on the order of 1000 whereas ultrasonic imaging the TBP must be orders of magnitude smaller [8]. In addition, the radar problem is often one of detection whereas ultrasound is a mapping of scatterers. Moreover, tight constraints on filters are imposed to reduce the possibility of artifacts generated by self-noise of the coded excitation/pulse compression system. The method of compression used dictates the eSNR, the maximum sidelobe levels, and the compressed pulse length. Sidelobes are a byproduct of pulse compression that can degrade image quality by returning on-axis echoes, which appear as ghost images. Conventional pulsing schemes do not suffer from sidelobes. If not carefully constructed, sidelobes from pulse compression of codes can be as high as 13.2 dB (sidelobes of the sinc function). A reasonable expectation is to require maximum range sidelobe levels to be lower than the dynamic range of the ultrasonic imaging system, which typically operates at dynamic ranges greater than 45 dB [20]. Misaridis and Jensen claimed to achieve range sidelobe suppression between 60 to 100 dB [16]. The method used to achieve such low sidelobe suppression was amplitude or phase pre-distortion in addition to mismatch filtering.

Several researchers have investigated coded excitation/pulse compression techniques for ultrasonic imaging systems with promising results [15]-[17], [20]-[24]. The most common waveforms in this class of signals are phase modulation (PM), linear frequency modulation (LFM), and nonlinear frequency modulation (NLFM) signals. A class of phase modulation codes of interest is the minimum peak sidelobe biphase codes called Barker codes [13]. Barker codes are a class of codes that modulate a pulse at

either 0 or 180 degrees. A correlation detector is used to extract and restore spatial resolution, i.e. a matched-filter. Barker codes are optimized for minimum sidelobes upon compression. However, only barker codes of length 1, 2, 3, 4, 5, 7, 11, and 13-bit are known, which restricts the time average transmit energy [13]. The sidelobe levels of an N-bit barker sequence can be approximated as 1/N [10]. In 2009, Xiang Lei et al. used a 13-bit Barker code to improve sensitivity of emboli detection in transcranial Doppler ultrasound [25]. Lei et al. cited a low eSNR in the cerebral artery as a reason to explore Barker codes because increasing peak pressure would increase the risk of cavitation.

One major drawback to Barker codes is the 13-bit limit. One coded excitation method to transmit longer codes with low sidelobe levels is to transmit complementary codes or Golay codes. Golay codes, by definition, consist of two waveforms and the sum of each waveform's respective autocorrelation function is zero everywhere except for the zero lag term [26]. Golay codes' two distinctive disadvantages are the need to transmit two coded pulses and the lag between the two pulses. The need to transmit two pulses reduces frame rate and, because of the time lag between pulses, Golay codes are better suited to imaging stationary targets. Takeuchi also proposed the use of Golay codes in medical ultrasound in 1979 with a 16-bit Golay pair [15], [27]. Takeuchi also proposed that the gain in eSNR from coded excitation would allow ultrasound imaging systems to migrate to higher frequencies, further increasing spatial resolution, or to decrease center frequency and/or to reduce ultrasonic exposure [15]. In other words, using coded excitation, the same eSNR as pulsing could be achieved by transmitting a lower peak amplitude signal, reducing ultrasonic dosage.

Coded excitation waveforms in ultrasound can be optimized to produce improved

image quality. A few desirable characteristics of an ultrasound waveform before compression are a large time-bandwidth product, short-duration, and low sidelobes upon compression. However, an excitation waveform of significantly longer duration is still undesirable because it can reduce frame rate, and the excitation pulse can overlap with echo returns. The frame rate can be reduced because as the pulse length is significantly extended, the interpulse interval (pulse repetition frequency or PRF) must also be extended. A reduction in the PRF will directly reduce frame rate.

1.2.5 Resolution Enhancement Compression

The resolution enhancement compression (REC) technique is a novel coding technique that improves not only the eSNR but also axial resolution [21]. The traits of the REC technique may be desirable for improving the detection of small lesions. Transducers are a band-limited resonant structure. REC boosts energy in the transition bands corresponding to the transducer impulse response, consequently doubling the usable bandwidth, improving the resolution, and improving the eSNR. REC was observed to boost system bandwidth (-3-dB bandwidth) by as much as 100% over conventional pulsing techniques. In addition, REC improved eSNR and spatial resolution (measured with the modulation transfer function (MTF)) in simulations and experiments [21]. The MTF quantifies how well an imaging system delivers contrast at different spatial frequencies. Furthermore, long range sidelobe levels were reported to be -45 dB.

The REC technique was also combined with frequency compounding (FC) to increase the tradeoff between spatial resolution and contrast [22]. Frequency compounding is a method of averaging images created from partially uncorrelated

subbands to reduce speckle interference and increase contrast. However, it also degrades axial resolution because each subband is a fraction of the original bandwidth. By combining REC with FC, contrast was improved by reducing speckle variance while maintaining the original bandwidth of the imaging system. Sanchez and Oelze claimed to achieve increases in CNR by as much as 231% over CP with subbands of 50% of the original transducer bandwidth [22].

In addition, the REC technique was also combined with quantitative ultrasound (QUS) imaging to estimate the effective scatterer diameter [23]. This technique, called REC-QUS, increased contrast of scatterer diameter images by 51%. In addition, REC-QUS decreased the standard deviation of effective scatterer diameter estimates by 60% in simulations. In experiments, REC-QUS was observed to reduce the standard deviation of effective scatterer diameter estimates by 34% to 71%.

In this study we propose to quantify the ability of an ultrasonic imaging system to detect small lesions when using REC. The boost in bandwidth and the increase in eSNR provided by the REC scheme should result in improved detectability of small lesions. Simulations and experiments were conducted to quantify the performance or REC for this task.

1.3 Organization of Study

This study is organized as follows. Chapter 2 outlines the resolution enhancement compression (REC) techniques, equipment used, and simulation methods. Chapter 3 presents a study on the limitations of REC with respect to maximum voltage that can be applied or maximum output pressure allowed. The goal was to determine if the limiting

factor in REC performance was applied voltage or output pressure. A higher output pressure will necessarily result in a higher eSNR, but the pressure levels are regulated by the FDA. The voltage levels that can be applied to a transducer are limited by the breakdown voltage of the material. Chapter 4 studies the effect of REC on small lesion detection as quantified by the lSNR metric. Lastly, Chapter 5 concludes the results of both studies.

Chapter 2 Methods

2.1 REC

The coded waveform that is transmitted can be crafted to optimize certain system properties. REC is a method of coded excitation that optimizes the coded waveform in terms of axial resolution. The axial resolution of an ultrasound imaging system is inversely proportional to the bandwidth of the transducer. When using a conventional pulsing scheme, the transducer is excited with a voltage impulse. The impulse response of the transducer dictates the shape of the emitted pulse and the bandwidth of the emitted pulse. Thus, even though the axial resolution is inversely proportional to bandwidth, only a finite bandwidth is available.

REC is a coded excitation/pulse compression scheme that boosts the energy in the transition bands of the transducer. The bandpass nature of the transducer normally attenuates frequencies in the transition band. By boosting the energy in the transition band with respect to the center frequency of the transducer, a larger usable bandwidth can be achieved. This boost in the transition bands is illustrated in Figure 2.1. A physical description of REC is the boosting of the frequencies on the edges of the transducer spectrum. The result is a higher useable bandwidth that is far enough above the noise floor for imaging.

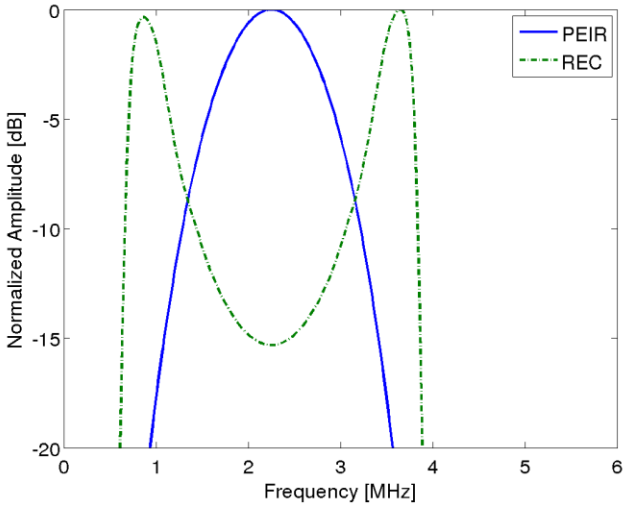

Figure 2.1. Transducer pulse/echo impulse response (PEIR) and a REC excitation waveform.

Consider the impulse response of a bandlimited transducer to be $h_1(t)$ and a desired impulse response, $h_2(t)$, of a second hypothetical transducer with a larger fractional bandwidth than $h_1(t)$. Let $v_{lin}(t)$ be a LFM chirp matched to the desired impulse response, $h_2(t)$, and let $v_{pre}(t)$ be a yet to be determined pre-enhanced chirp used to excite the actual transducer having the impulse response, $h_1(t)$. The output of a transducer excited with a code is the coded waveform convolved with the impulse response. Let $c_1(t)$ and $c_2(t)$ represent the output of these respective convolutions,

$$\begin{bmatrix} h_1(t) & 0 \\ 0 & h_2(t) \end{bmatrix} \begin{bmatrix} v_{pre}(t) \\ v_{lin}(t) \end{bmatrix} = \begin{bmatrix} c_1(t) \\ c_2(t) \end{bmatrix}. \tag{2.1}$$

By setting $c_1(t)$ and $c_2(t)$ equal, the pre-enhanced chirp can be solved for by applying the theory of convolution equivalence to the following system:

$$h_1(t) * v_{pre}(t) = h_2(t) * v_{lin}(t). \tag{2.2}$$

By solving Equation (2.2**)** in the frequency domain, the convolution becomes a multiplication and solving for the pre-enhanced chirp can be simplified,

$$V_{PRE}(f) = \frac{V_{LIN}(f) \times H_2(f)}{H_1(f)}. \tag{2.3}$$

To avoid dividing by zero a modified inverse can be used [21],

$$V_{PRE}(f) = V_{LIN}(f) \times H_2(f) \times \frac{H_1^*(f)}{|H_1(f)|^2 + |H_1(f)|^{-2}}. \tag{2.4}$$

In practice, the transducer will be excited by a pre-enhanced chirp found through convolution equivalence and then compressed with the linear chirp $v_{lin}(t)$, to obtain $h_2(t)$. Moreover, the desired impulse response, $h_2(t)$, can be constructed to have properties desirable for an imaging system such as a large fractional bandwidth. Figure 2.2 shows this sequence in the time domain.

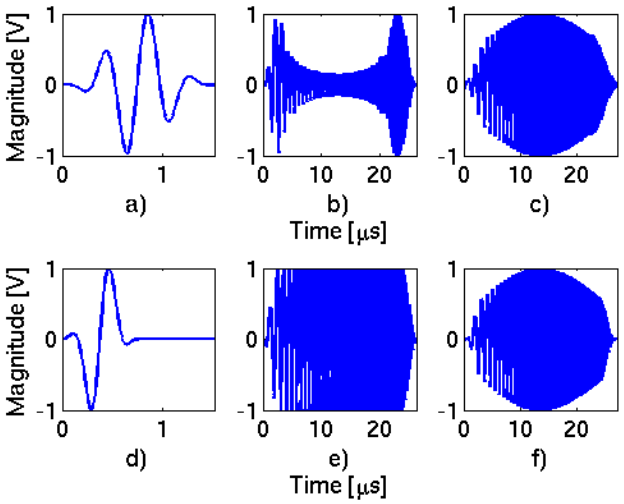

Figure 2.2. Convolution equivalence: (a) pulse-echo impulse response with 48% fractional bandwidth, (b) pre-enhanced chirp, (c) convolution of pulse-echo impulse response and pre-enhanced chirp, (d) desired pulse-echo impulse response of 96% fractional bandwidth, (e) linear chirp, and (f) convolution of 96% fractional bandwidth source and the linear chirp.

The impulse response convolved with a pre-enhanced chirp (Figure 2.2c) is equivalent to the desired impulse response convolved with the linear chirp (Figure 2.2f) by convolution equivalence. Therefore, if the actual transducer is excited by a pre-enhanced chirp a compression method can be designed with $v_{lin}(t)$ that will result in a

higher bandwidth imaging system. The linear chip is matched to a transducer impulse response by setting the bandwidth of the linear chip to the optimum bandwidth of the transducer, i.e., defined as 1.14 times the -6 dB bandwidth of the transducer [24]. A linear chirp can be expressed as [16]

$$v_{lin}(t) = w(t)\exp\left\{j2\pi\left[\left(f_0 - \frac{B}{2}\right)t + \frac{B}{2T_P}t^2\right]\right\}, 0 \le t \le T_P, \tag{2.5}$$

where f_0 represents the center frequency and B/T represents the FM sweep or frequency ramp constant. The parameter B represents the total bandwidth that will be swept, which is $[f_0 - B/2, f_0 + B/2]$, and $w(t)$ is a windowing function. The parameter T_P is time period of the chirp. The FM linear chirp can be represented in discrete frequency as

$$v_{lin}[n] = w[n]\exp\left\{j2\pi\left[\left(f_0 - \frac{B}{2}\right)\frac{n}{f_s} + \frac{B}{2T_P}\left(\frac{n}{f_s}\right)^2\right]\right\}, 0 \le n \le {T_P}/{f_s}. \tag{2.6}$$

In Equation (2.6) the continuous parameter t has been replaced by the discrete integer n and f_s represents the sampling frequency. The window function, $w[n]$, is a pre-transmission smoothing parameter that helps lower range lobes upon compression. The windowing function used was the Tukey window with 8% taper [21]

$$w[n] = \begin{cases} 1, & 0 \le |n| \le \dfrac{N}{2}[1+\alpha] \\ 0.5\left[1.0 + \cos\left(\pi \dfrac{\mathrm{n} - \dfrac{\mathrm{N}}{2}[1-\alpha]}{N[1-\alpha]}\right)\right], & \dfrac{N}{2}[1+\alpha] \le |n| \le N. \end{cases} \tag{2.7}$$

The parameter α controls the amount of taper which varies from 0 to 1, representing a rectangular window and a Hanning window, respectively. Without a windowing function the sidelobes approach that of the sinc function at -13 dB. A Hanning window greatly improves sidelobes, i.e., down to -46 dB, but greatly broadens the mainlobe. The Tukey

window allows a tradeoff between spreading of the main lobe and sidelobe suppression.

To restore the axial resolution the echo must be post-processed by pulse compression. The naïve approach to this deconvolution problem is the inverse filter. This approach amplifies noise and is therefore impractical. The matched filter, which maximizes eSNR, suffers from large sidelobes, even as high as -13 dB if not properly constructed. A compromise between inverse filtering and matched filtering is Wiener filtering [17]. Pulse compression in the REC technique is achieved through a Wiener filter design. The Wiener filter used in the REC technique is given by

$$\beta_{REC}(f) = \frac{V'^{*}_{LIN}(f)}{\left|V'_{LIN}(f)\right|^2 + \gamma \overline{\mathrm{eSNR}}^{-1}(f)}. \tag{2.8}$$

The compression filter in Equation (2.8**)** allows a trade-off between gain in eSNR and sidelobe levels. The γ parameter is a smoothing parameter, a tunable constant that allows the selection of where the filter should operate, i.e., closer to an inverse filter or to a matched filter. The $V'_{LIN}(f)$ term is the frequency domain representation of the linear chirp used in the convolution equivalence. The $\overline{\mathrm{eSNR}}$ term is a measurement of noise per frequency channel and was estimated by [28]

$$\overline{\mathrm{eSNR}}(f) = \frac{|H_{2c}(f)|^2 \times \mathrm{E}\{|\mathrm{F}(f)^2|\}}{E\{|\eta(f)|\}}, \tag{2.9}$$

where $F(f)$ is the object function, $\eta(f)$ is the frequency spectrum of the noise, and $H_{2c}(f)$ is the frequency domain equivalent of

$$h_{2c}(t) = \mathrm{E}\{\mathrm{g}(t)\}. \tag{2.10}$$

The parameter g*(t)* is the compressed signal over noise. Optimal sidelobes and spatial resolution occur when the filter is closer to an inverse filter.

The $e\overline{SNR}$ (defined in Equation (2.9)) is shown in Figure 2.3 for a low noise situation. The $e\overline{SNR}$ term shapes the compression filter to reject out-of-band noise while boosting signal power in the passband of the transducer. The $e\overline{SNR}$ for the CP is plotted for reference only as no post-processing of the CP is performed.

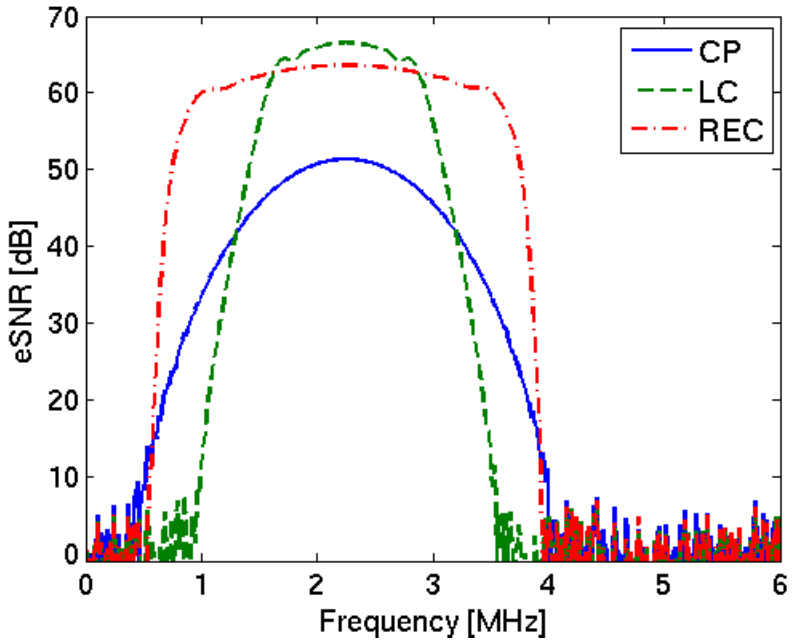

Figure 2.3. $e\overline{SNR}$ of CP, LC, and REC.

The effect on the filter of the LC and REC $e\overline{SNR}$ can be discerned by reference to Equation (2.8). As the signal power dominates the $e\overline{SNR}$ term, such as the passband of the transducer, the inverse of $e\overline{SNR}$ is driven to zero. Equation (2.8) then reduces to

$$\beta(f) = \frac{1}{V'_{LIN}(f)}, \tag{2.11}$$

or what would at first glance appear to be an inverse filter for a source excited with a linear chirp. However, because the source was actually excited with a pre-enhanced chirp, the filter is actually a mismatched filter that results in an increased bandwidth. The converse case occurs at the edges of the passband and outside of the passband where

$e\overline{SNR}$ is low. A low $e\overline{SNR}$ translates into a large constant in the denominator of the filter effectively becoming a scale factor, not affecting the filter characteristics. This filter could be represented as

$$\beta\ (f) = \frac{V'^{*}_{LIN}(f)}{M}, \tag{2.12}$$

where M is a large number. Equation (2.12) behaves as a matched filter boosting eSNR.

2.2 Tunable Constant

The tunable constant in Equation (2.8) is a scalar that allows the user/system to adjust the overall behavior of the compression filter. The parameter γ can be thought of as a manual lever to control if the compression filter is operating closer to an inverse filter or closer to a matched-filter. No optimization of the γ parameter was considered in this study. However, the filter characteristics are shown for the three excitation types in Figure 2.4. The gain of the excitation waveforms trails off at high eSNR because of ringing artifacts. These artifacts are not present in CP because no post-processing is necessary. A quick conclusion can be drawn from Figure 2.4, that above a certain eSNR threshold, no gain in eSNR can be achieved by coded excitation. Coded excitation performs best in higher noise situations and when γ is high (10^6 for high gain) with respect to eSNR.

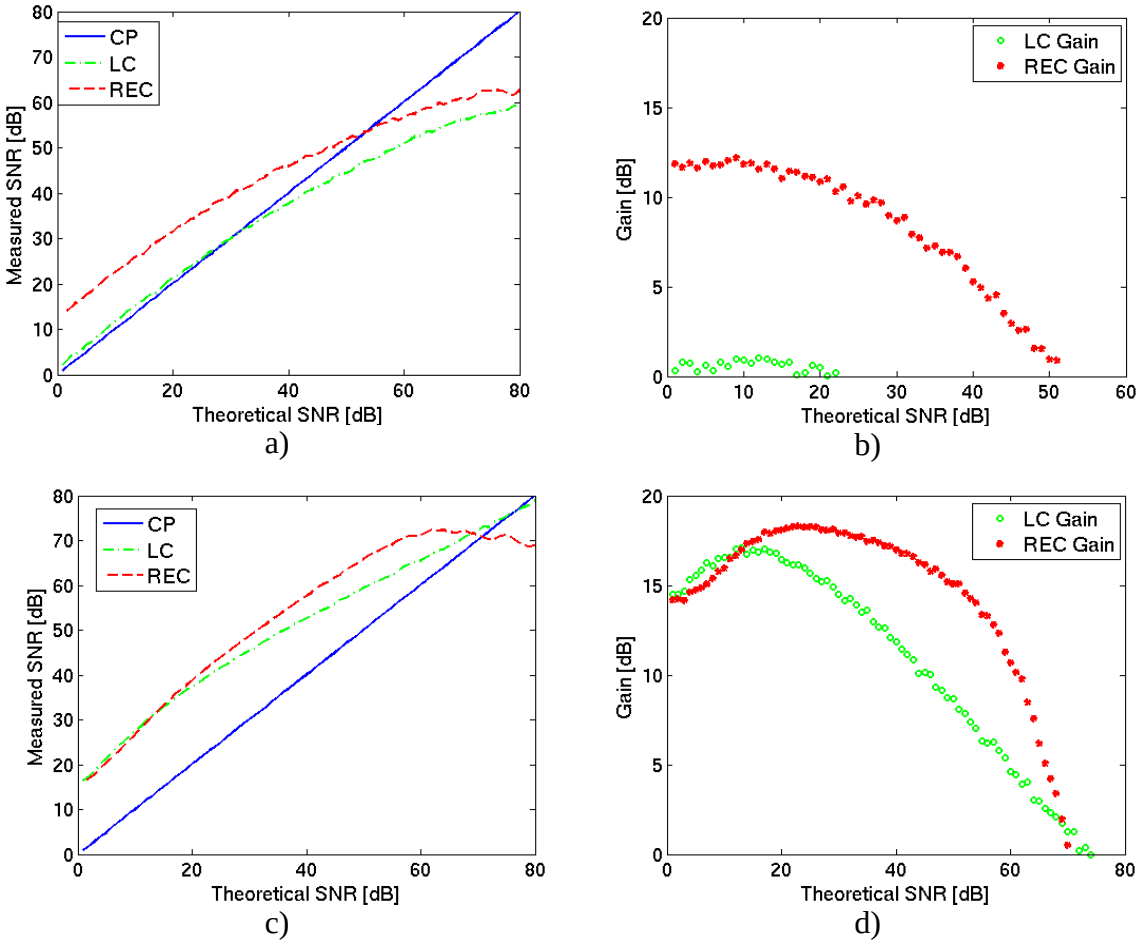

Figure 2.4. Effects of γ on Wiener filter eSNR and gain (a) eSNR with $\gamma = 10^2$, (b) gain with $\gamma = 10^2$, (c) eSNR with $\gamma = 10^6$, (d) gain with $\gamma = 10^6$.

The ringing, observed in Figure 2.5a, when eSNR is very high is the point where sidelobes dominate. A close-up of the ringing in the time-domain is shown in Figure 2.5b.

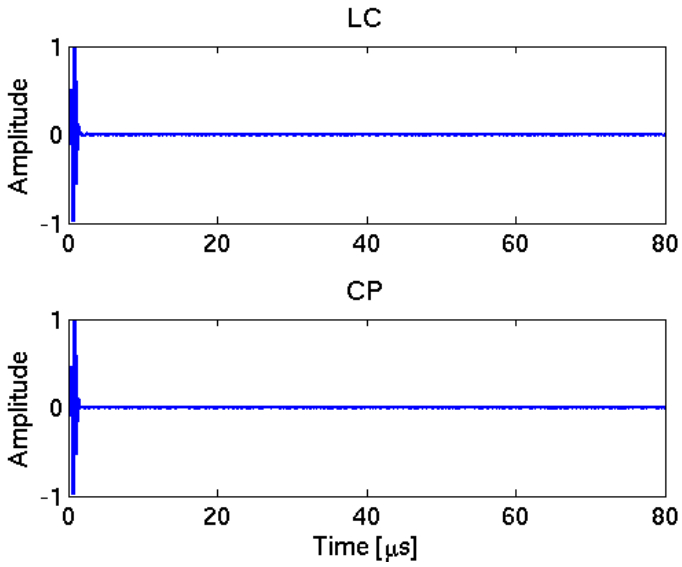

a)

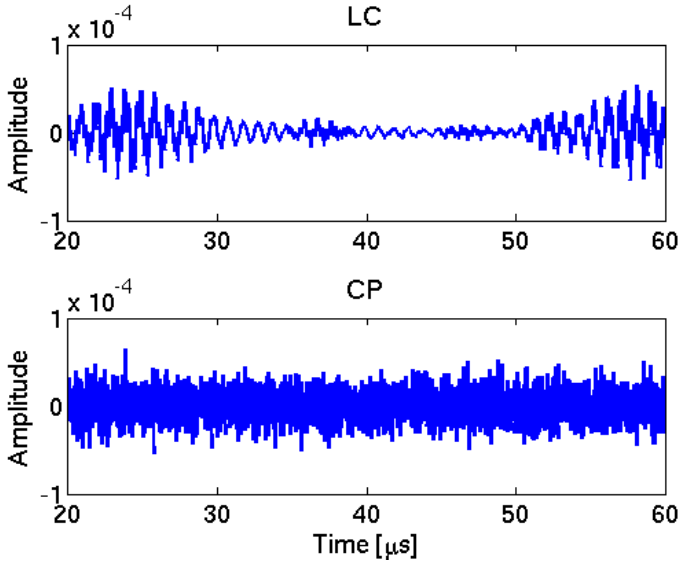

b)

Figure 2.5. Ringing (sidelobes) (a) LC and CP, (b) a close-up of 20-60 μs.

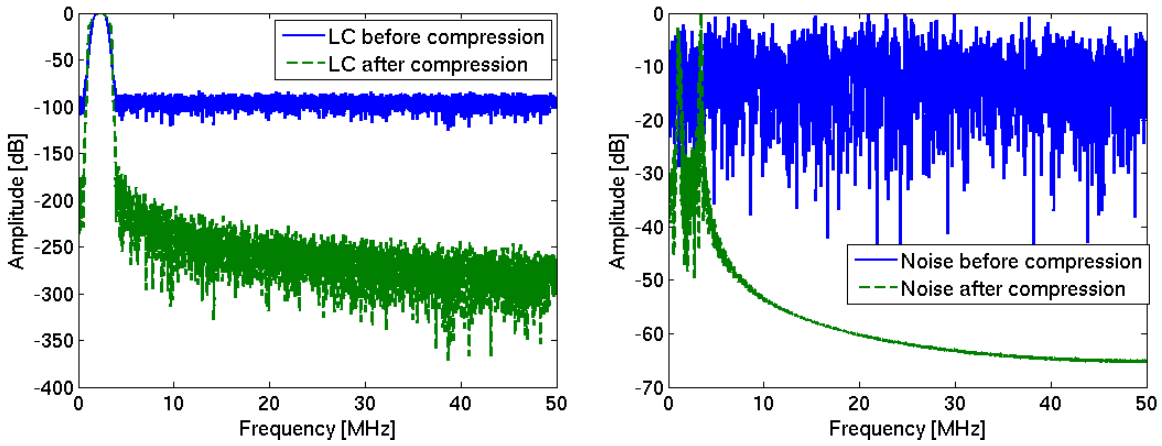

a) b)

Figure 2.6. (a) LC power spectrum before and after compression of a high eSNR case, (b) power spectrum of only noise of LC signal before and after compression.

The ringing artifacts of the LC corrupt the measurement of eSNR. This is further validated by Figure 2.6a and b which illustrate the power spectrum of the LC case. The LC normalized power spectrum before compression and after compression (Figure 2.6a) show signal power in the 2.5 MHz range and a very low noise power after compression (consistently lower than 200 dB). A normalized power spectrum of noise (Figure 2.6b) also validates the ringing as before. Sharp peaks near the center frequency of the transducer are sure to be the time-domain ringing.

The effect of the tunable parameter, γ, on the sidelobe levels and axial resolution can be seen in Figure 2.7 and Figure 2.8. A low value of γ ensures that sidelobe levels will be below 30 dB for REC (Figure 2.7, $\gamma = 10^{-2}$). However, larger values of γ could severely affect sidelobe levels (Figure 2.8, $\gamma = 10^{6}$). Also notice how the main lobe for both coded excitation techniques broadened slightly with the increase in γ. The broadening of the main lobe and interference caused by sidelobes degrades axial resolution and performance. In terms of axial resolution, a lower value of γ is preferred to reduce sidelobe levels and to minimize main lobe width. This is the trade-off between

eSNR gain and axial resolution that must be balanced to preserve image quality and fidelity.

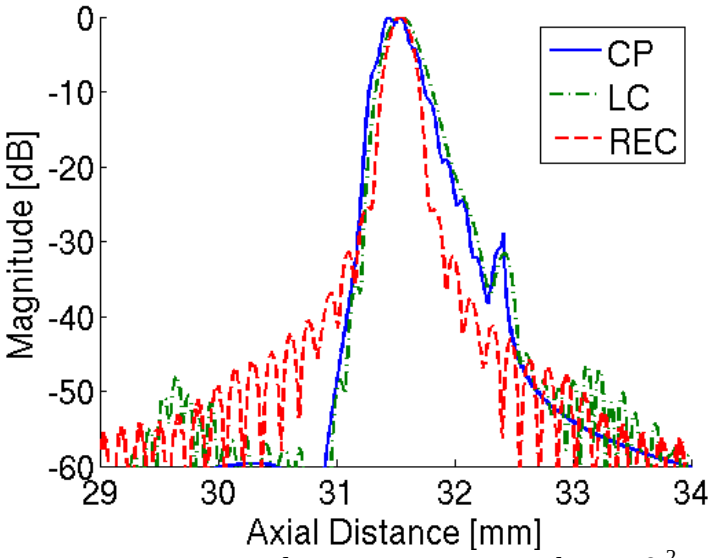

Figure 2.7. Envelope compression with $\gamma = 10^{-2}$.

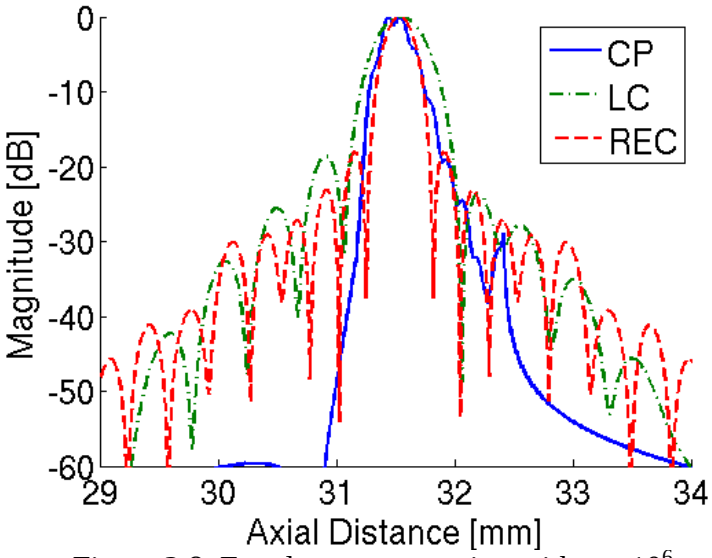

Figure 2.8. Envelope compression with $\gamma = 10^{6}$.

2.3 Quality Metrics

To evaluate the performance of small lesion detection using the REC technique the following image quality metrics were used in simulations and experiments:

1. Modulation transfer function (MTF): The MTF quantifies the imaging system's ability to deliver contrast at different spatial frequencies, i.e., it quantifies the spatial resolution of the imaging system. The MTF is defined by [29]:

$$\mathrm{MTF}(k|\mathbf{x}) = \frac{|H(k|\mathbf{x})|}{|H(0|\mathbf{x})|}. \tag{2.13}$$

The axial resolution is defined from when the *k* value falls below some threshold, e.g., in this work it is the *k* value, k_0, where the amplitude falls to 0.1 of its maximum value. The spatial resolution can then be calculated as follows:

$$\lambda_{res} = \frac{1}{2}\frac{2\pi}{k_0}\,(\mathrm{m}). \tag{2.14}$$

Figure Figure 2.9 shows the MTF for the REC technique and reveals how using REC resulted in improved axial resolution [21].

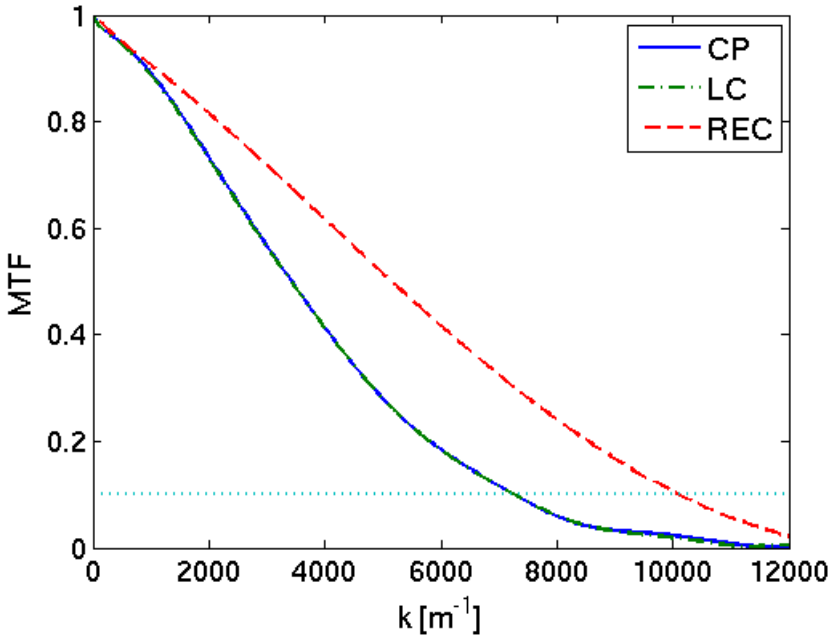

Figure 2.9. The modulation transfer function (MTF). The resolution of a system can estimated as when the value of the MTF falls below some threshold, here the threshold has been set to 0.1.

2. Contrast-to-noise ratio (CNR): CNR is a metric that quantifies the perceived difference between a target image and its background. CNR is defined in this work as [12]

$$\mathrm{CNR} = \frac{|\langle S_i \rangle - \langle S_o \rangle|}{\sqrt{\sigma_i^2 + \sigma_o^2}}, \tag{2.15}$$

where $\langle S_i \rangle$ and $\langle S_0 \rangle$ represent the average intensity inside and outside the target, respectively, and σ_i^2 and σ_0^2 represent the variance inside and outside the target, respectively. To calculate the CNR, the mean and variance of the signal inside the lesion was estimated by a circular region 90% of the size of the lesion. The mean and variance of the background was estimated by calculating the mean and variance of a disk shaped region surrounding the inclusion. A small buffer region

between the lesion and background was included to ensure that only target or background points were included.

3. Echo signal-to-noise-ratio (eSNR): For this work eSNR was calculated by taking the variance of a collection of points near the focus and dividing it by an estimate of the noise power. The noise power was estimated by taking the variance of the radio frequency (RF) time signal corresponding to the water bath before the phantom. The assumption here was that the noise power was constant throughout the RF data. The signal variance decayed to the noise variance as samples were taken deeper with respect to axial distance due to attenuation. The eSNR was calculated pre and post compression to estimate the gain in eSNR due to the coding technique. Assuming matched filtering, the predicted gain in eSNR relative to pulse compression should be on the order of the time-bandwidth product (TBP) [20].
4. Resolution cell size: Wagner et al. demonstrated that the average resolution cell size was related to the average speckle cell size [11]. The resolution cell size was estimated from both the physical properties of the transducer and the characteristics of speckle. The speckle cell size was found through the autocovariance function. Furthermore, the axial speckle cell size is inversely proportional to pulse bandwidth and proportional to transducer beamwidth [6]. Thus an estimate of the resolution cell volume (axial resolution, S_{cz}, and lateral resolution, S_{cx}) using 2^{nd} order statistics can be made with the autocorrelation function. The M point 2-D autocorrelation for a discrete process at lag k and l is represented as [8]

$$R_{ff}(k,l) = \sum_{m=0}^{M-1} f_{m,n} f_{m+k,n+l}, \tag{2.16}$$

where f_{mn} represents the original RF data from the region. The autocorrelation function was applied to a region of speckle adjacent to the lesion in both simulated and experimental data. In the lesion detection simulation and experiments, a 2x2 cm^2 square region of interest was used to estimate the resolution cell size from the speckle. The region of interest was located at the focus axially and to the far left of the image laterally. For comparison, an estimate of the resolution cell size in the lateral direction based on the transducer physical properties can be estimated as [30]

$$S_{cx}^{'} = \frac{0.87\lambda z_0}{d'}, \tag{2.17}$$

where z_0 is the distance to the focus, d' the diameter of the transducer divided by 1.08, and λ is the wavelength of sound in the medium. The substitution $d' = d/1.08$ was recommended by Wagner et al. for piston transducers [11]. An estimate of the axial resolution is defined by

$$S_{cz}^{'} = \frac{1.37}{\Delta f}, \tag{2.18}$$

where Δf is the -6-dB bandwidth in MHz and $S_{cz}^{'}$ has units of mm.

5. Lesion signal-to-noise-ratio (lSNR): lSNR is an estimate of an isolated observer to detect a lesion and can be estimated by [6]

$$l\text{SNR} = \frac{\text{CNR} \times d}{\sqrt{S_{cx} \times S_{cz}}}. \tag{2.19}$$

This metric depends on the lesion diameter, d, which is known *a priori* and S_{cx} and S_{cz} are the axial and lateral estimate of the resolution cell volume based on the

speckle characteristics. The importance of this metric is that it includes not only the contrast of the lesion but also the ratio of the lesion size to the spatial resolution of the imaging system.

2.4 Voltage versus Pressure Limited REC Study

This study incorporated four different excitation waveforms (Figure 2.10a-d); the conventional pulse (CP), the linear chirp (LC), REC pressure limited (REC PL), and REC voltage limited (REC VL). Not shown in Figure 2.10 is the pulse/echo impulse response used. The pulse/echo impulse response had a center frequency of 2.35 MHz and a -3-dB bandwidth of 1.22 MHz which corresponds to a fractional bandwidth of 52%. The CP is shown in Figure 2.10a. Note that the maximum pressure at the focus will be proportional to 1 Pa. Figure 2.10b shows the excitation of the LC (left) and the output after convolution with the transducer pulse/echo impulse response (right). The TBP of the LC was 36.5 and the expected gain in eSNR between pre and post-compression was 15.6 dB. Figure 2.10c shows the pressure limited REC excitation. In this case, the assumption is that the system is pressure limited and that the transducer can be driven as hard as needed to achieve the same pressure at the focus as CP and the LC. Figure 2.10a-c represent systems that are limited by pressure at the focus. However, if the system is voltage limited a different chirp must be used for the REC technique. The voltage limited pre-enhanced chirp was solved limiting the simulated excitation voltage between $\pm$ 1 V, left side of Figure 2.10c. The scaled down voltage limited chirp and the output after convolution with the pulse/echo impulse response are shown in Figure 2.10d. Both pre-enhanced chirps, voltage limited and pressure limited, have the same TBP of 70.3 which

should translate into a pre to post-compression gain of 18.5 dB. The final eSNR of the pressure limited case should be better than the voltage limited case because a higher pressure at the focus directly translates into a higher eSNR. Determining how this will affect lSNR is the purpose of this study.

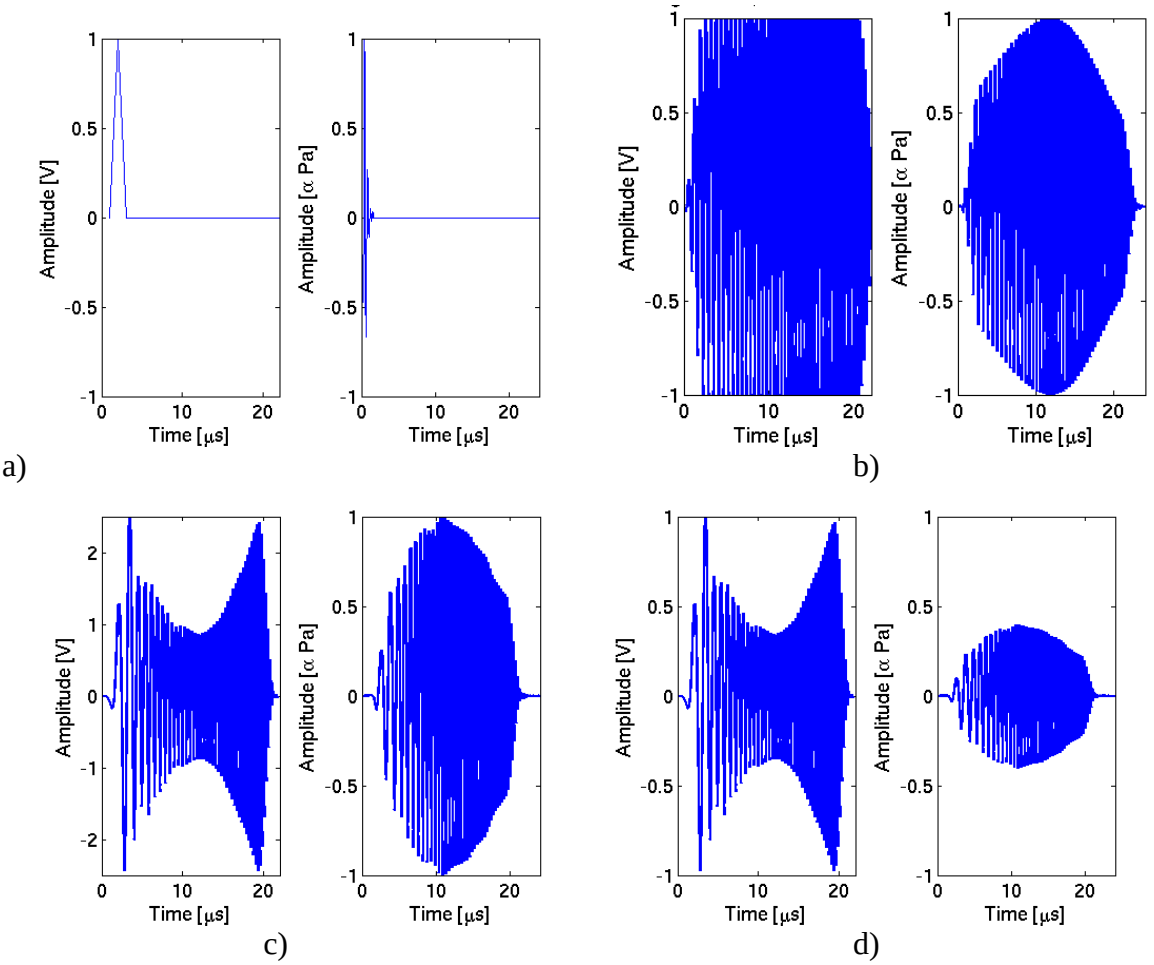

Figure 2.10. (a) left: CP, right: CP after convolution with PE/IR, (b) left: LC of TBP 36.5, right: LC after convolution with PE/IR, (c) left: pressure limited pre-enhanced chirp, right: pressure limited pre-enhanced chirp after convolution with PE/IR, and (d) left: voltage limited pre-enhanced chirp, right: voltage limited pre-enhanced chirp after convolution with PE/IR.

2.4.1 Simulations for Voltage versus Pressure Limited REC Study

A MATLAB add-on called FIELD II that simulates ultrasound pressure fields was used to test the different excitation schemes [30], [31]. FIELD II uses a far-field

approximation based on the transducer geometry and impulse response which is defined by the user. FIELD II is based on the Tupholme-Stephanishen model [30]. However, FIELD II does not incorporate frequency dependent scattering. To compensate for scattering an f^2 filter was used on all RF data from FIELD II.

In simulations, a total of 150 software phantoms were generated with lesion diameters ranging in size between 0.5 and 8.0 mm. Ten trials at each lesion diameter size were simulated. Field II was then used to generate RF data for the four excitation methods from the software phantoms. The resulting simulated B-mode images were compared using lSNR, eSNR, and CNR. The purpose of the simulations was to determine how well the voltage limited chirp performed with respect to the other excitation methods in detecting lesions.

2.5 Small Lesion Detection Study

2.5.1 Simulations for Small Lesion Detection Study

The different excitation schemes were convolved with a theoretical transducer impulse response. The outputs were then normalized to ensure that the peak pressure amplitudes at the focus of the simulated source were the same for all the different excitation schemes. Noise was then added pre-compression and the coded waveforms were compressed. Three pulsing schemes were compared: conventional pulsing (CP), the conventional linear chirp (LC), and the pre-enhanced chirp (REC). The simulated source was taken from the actual PEIR of an f/2.66 transducer with a center frequency of 2.35 MHz. The PEIR was estimated by measuring the reflection off of a Plexiglas plate located at the focus.

As in the simulations in Section 2.4, Field II was used to simulate RF data. A total of 150 phantoms were simulated with lesion diameters ranging between 0.5 and 8.0 mm. Again, simulated phantoms with circular lesions were constructed which contained scatterers placed spatially at random positions and uniformly throughout the phantoms at a concentration of 15 scatterers per resolution cell volume. The mean scattering strength of the scatterers inside the lesion was either -12 dB or +6 dB with respect to the scatterers outside the lesion. Phantoms were simulated with lesion sizes ranging from 1 to 8 mm in diameter in increments of 0.5 mm. Ten phantoms for each lesion size were simulated. The images produced using the three different excitation methods were then compared using CNR, lSNR, eSNR metrics, and estimated speckle cell volume based on the autocorrelation function. To estimate the gain in eSNR, both pre and post-compression estimates of the eSNR were made of the LC and REC waveforms. All RF data were envelope detected with the Hilbert transform and log compressed. The dynamic range for all images was hard limited to 60 dB. Any values lower than -60 dB were truncated to -60 dB. A dynamic range of 60 dB spanned the range of the RF data. A much higher dynamic range, for example, such as 100 dB, would result in a "washed out" or an over compressed image. No data would have been lost but the display range would have been over compressed with respect to the dynamic range present in the RF data. The numerical values of the CNR calculations would be different. However, as log compression is a one-to-one mapping function, the overall trends in CNR would be preserved. It the data were compressed on a 30 dB dynamic range, many values in the image would be truncated and set to -30 dB because the RF data had a larger dynamic range than 30 dB. In this case, the image would be corrupted by throwing away too

much data. Even so, a CNR value would probably be higher, given that the lesion-to-background strength was less than 30 dB and a 30 dB dynamic range would spread the numerical values of CNR computed. Adjusting the dynamic range of the "system" serves as a sort of contrast knob on a television set. The overall trends between the different excitation techniques will be preserved even though a specific value of CNR would be different.

2.5.2 Experimental Setup for Small Lesion Detection Study

The experimental setup is shown in Figure 2.11a and b. The experimental setup included a single-element, weakly focused (f/2.66) transducer (Panametrics, Waltham, MA). This represents a fixed focus system. Only images produced near or at the focus are considered in this study. The transducer center frequency (measured) was 2.35 MHz and had a -3-dB pulse-echo fractional bandwidth of 52%. The transducer was mounted on a positioning system that mechanically translated the transducer perpendicular to the major axis of a cone phantom. Two different setups were used: (1) the CP system and (2) the REC/LC system. Different electronic equipment produced different noise levels. The two different systems are described on the following page.

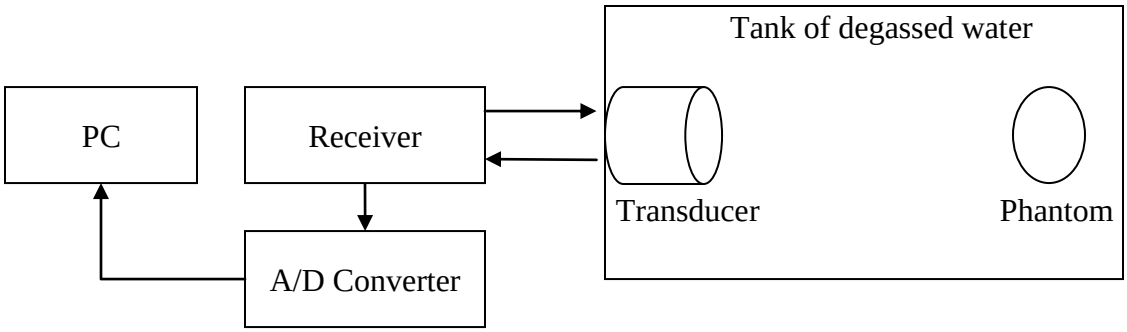

a)

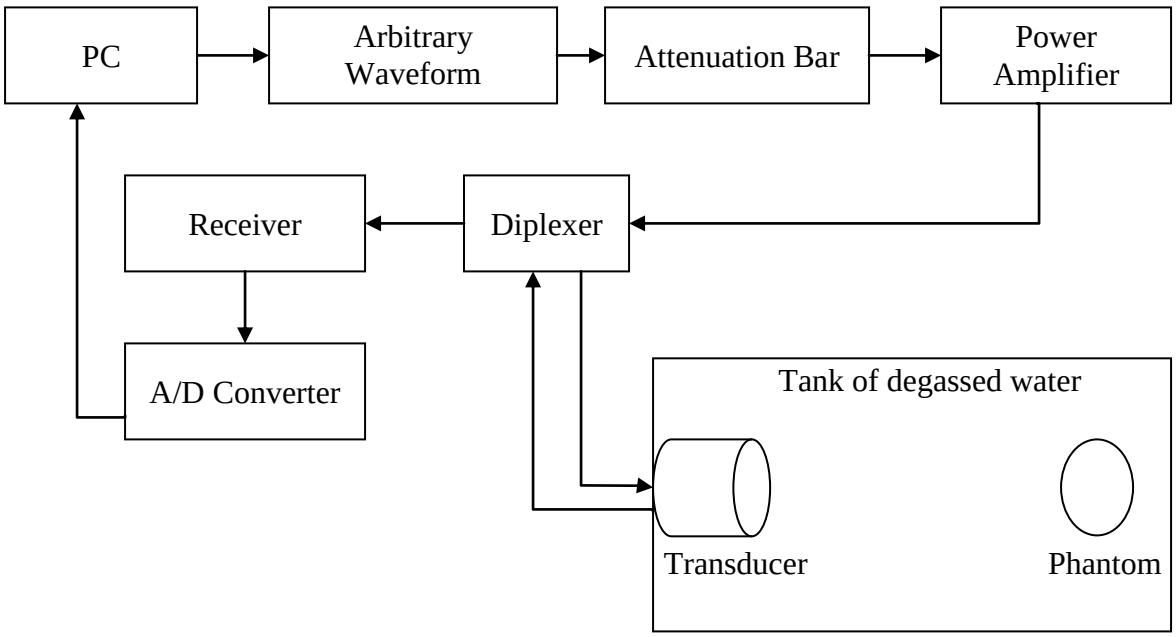

b)

Figure 2.11. Experimental setup for coded waveforms (a) conventional pulse (CP), (b) linear chirp (LC) and REC setup.

1. The CP system: A pulser-reciever (Panametrics 5800, Waltham, MA) was used to excite the transducer and receive the echoes. The echoes were then digitized at 100 MHz with a 12-bit A/D card (Strategic Test Digitizing Board UF3025, Cambridge, MA). All further processing was completed in MATLAB.
2. The REC/LC system: The excitation waveform was designed in MATLAB and then downloaded to an arbitrary waveform generator (AWG) (Tabor Electronics

W128A, Tel Hanan, Israel) and amplified 50 dB (ENI 3251, Rochester, NY). However, the output of the waveform generator was set at 2 V peak-to-peak even though the input to the 50 dB power amplifier was limited to 1 V_{rms}. The noise floor of the arbitrary waveform generator was the same whether the output was set to 1 V peak-to-peak or 2 V peak-to-peak. To achieve maximal suppression of the noise floor, peak-to-peak output of the AWG was set to 2 V peak-to-peak. A sin wave of 2 V peak-to-peak is $^{2V}/_{\sqrt{2}}$ or about 1.41 V_{rms}. The 1.41 V_{rms} output was then passed through the attenuation bar set at 9 dB of attenuation. The output of the attenuation bar, 1.41 V_{rms}/2.82 (Equation (2.20)), would thus be 0.5 V_{rms} and under the 1 V_{rms} limit of the power amplifier. The 50 dB power amplifier was found to distort waveforms that were close to the 1 V_{rms} limit. This distortion was much reduced when input power to the amplifier was limited to 0.5 V_{rms},

$$\begin{aligned} P_{out}\,(\text{dB}) &= 20\log\frac{V}{V_{ref}} - 9\ \text{dB} \\ &= 20\log\frac{V}{V_{ref}} - 20\log 2.82 \\ &= 20\log\frac{{}^{V}/_{2.82}}{V_{ref}}. \end{aligned} \tag{2.20}$$

The amplified signal was passed through a diplexer (Ritec RDX-6, Warwick, RI) to the transducer. As in the CP system, the pulser-receiver was used to receive the echoes before being digitized by the same 12-bit A/D card. All post-processing was then completed in MATLAB.

A drawback about the two setups shown Figure 2.11 is that the noise floors are different for CP and the two coded techniques. The CP setup used in Figure 2.11a had a

different noise floor than the setup in Figure 2.11b. This is unavoidable as different equipment is used to produce and amplify conventional pulse generation than coded excitation. The result in experiments is that the noise floor for the coded waveforms was higher, a lower eSNR, than for conventional pulsing. Thus, comparing the two directly amounted to comparing a relatively noise free conventional pulsing system with a noisy coded excitation system. It is hypothesized that the lower baseline eSNR in the coded system was due to noisy amplifiers and extra electrical connections in the coded excitation steps. The conventional pulse setup, Figure 2.11a, only used two sets of connectors: one set for the receiver-transducer and a one-way connect between the receiver and the A/D converter. Every time the signal is passed between equipment, or even just over a wire for that matter, unwanted noise is added. In the absence of a more perfect setup, the noise floor between the two systems was normalized by adding white Gaussian noise to RF data with the setup shown in Figure 2.11a. In this manner, the eSNR or raw RF data from both setups was the same before further processing. To facilitate a comparison of systems with similar noise levels, the eSNR before compression was normalized to approximately 9.5 dB for both setups.

The cone to background contrast was fabricated to be +6 dB. This contrast was achieved by adding a different concentration of powdered graphite (Table 2.1 and Table 2.2). In addition, speed of sound of the phantom was estimated to be 1540 m/s with an attenuation of 0.49 dB MHz^{-1} cm^{-1} [32]. The cone phantom was scanned at slices that corresponded to a lesion diameter of approximately 3, 5, and 8 mm. Two waveforms were transmitted: a pulse, and the pre-enhanced chirp (Figure 2.12b). The desired impulse response had a center frequency of 2.19 MHz and a 104% -3 dB pulse-echo

fractional bandwidth. In this case, the REC technique doubled the fractional bandwidth of the actual impulse response of the transducer. By convolution equivalence in the previous section, Figure 2.12c and f should be the same. The REC compression filter is as described in Eq. (8), but the new desired impulse response, Figure 2.12d, was used to create the compression filter. The TBP of the pre-enhanced chirp (Figure 2.12b) was 70.3 and the TBP of the linear chirp (Figure 2.12e) was 63.4.

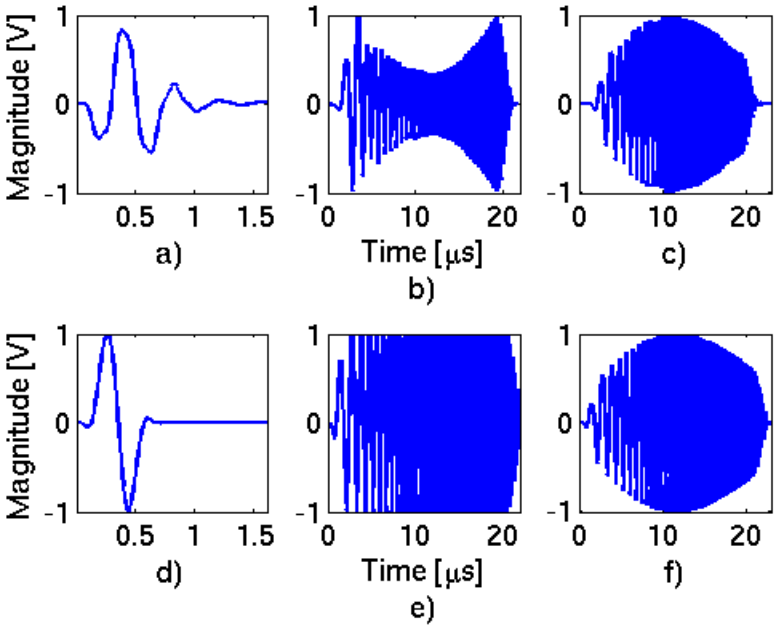

Figure 2.12. (a) Pulse/echo impulse response of transducer f_0 = 2.35 MHz and -3 dB fractional bandwidth of 52%, (b) pre-enhanced chirp, (c) the convolution of the PE/IR (a) and the pre-enhanced chirp (b), (d) Desired pulse/echo impulse response with f_0 = 2.19 MHz and a -3 dB fractional bandwidth of 104%, (e) linear chirp of optimum bandwidth, (f) convolution of desired impulse response (d) and linear chirp (e).

Table 2.1. Composition of the cone portion of the hydrogel phantom [32].

Material	**Percent**
Deionized water	83.4%
N-propanol	9%
Type-A gelatin (Fisher Scientific, Pittsburg, PA)	5.5%
Powdered graphite	2%
Formaldehyde	0.1%

Table 2.2**.** Composition of the medium surrounding the cone of the hydrodgel phantom [32].

Material	**Percent**
Deionized water	84.8%
N-propanol	9%
Type-A gelatin	5.5%
Powdered graphite	0.5%
Formaldehyde	0.1%

Lastly, a LC compression filter was set up to mimic a linear chirp. The RF data that were generated with the pre-enhanced chirp were not only compressed with the REC filter, but also with a filter based on the actual excitation signal, i.e., the pre-enhanced chirp. The REC technique requires a boost in bandwidth which is brought about by the coded waveform and compression with a higher bandwidth filter. Here, in addition to the REC compression, a compression was also carried out with the original chirp to mimic a conventional pulse compression scheme. This will not give the same boost in resolution but should give a respectable gain in eSNR while approximately maintaining axial resolution. The LC compression filter is as follows:

$$\beta_{LC}(f) = \frac{V_{PRE}^{*}(f)}{\left|V_{PRE}(f)\right|^{2} + \gamma\overline{\mathrm{eSNR}}^{-1}(f)}, \tag{2.21}$$

where $V_{\mathrm{PRE}}(f)$ is the frequency domain equivalent of the pre-enhanced chirp and $\mathrm{eSNR}^{-1}(f)$ was calculated as in Equation (2.9).

Chapter 3 Results:
Pressure versus Voltage Limited REC

3.1 Description of Study

To quantify the performance of REC when the source is peak voltage limited or peak pressure limited, four excitation waveforms were tested for their ability to image ultrasound lesions. The four waveforms were the conventional pulse (CP), the linear chirp (LC), REC pressure limited (REC PL), and REC voltage limited (REC VL). Image quality metrics were based on CNR, eSNR, and lSNR.

3.2 Results of Study

The results of CNR and lSNR for the 150 phantoms are shown in Figure 3.1a and b. REC VL outperformed the CP but did not equal the LC. Even as the lesion diameter decreased, the same overall trend was observed until a lesion size of about 2 mm. At this point CNR estimates of all techniques began to behave erratically. The smallest lesion of 0.5 mm shows what was surely an erroneous measurement. The 0.5 mm lesion only included 104 data points inside the region of interest to calculate CNR. The same trends were observed in the lSNR estimates (Figure 3.1b). Again, it is noted that lSNR includes the CNR. The superiority of the REC PL was clearly observed in the lSNR metric. However, it is a positive result that the REC VL outperformed the CP.

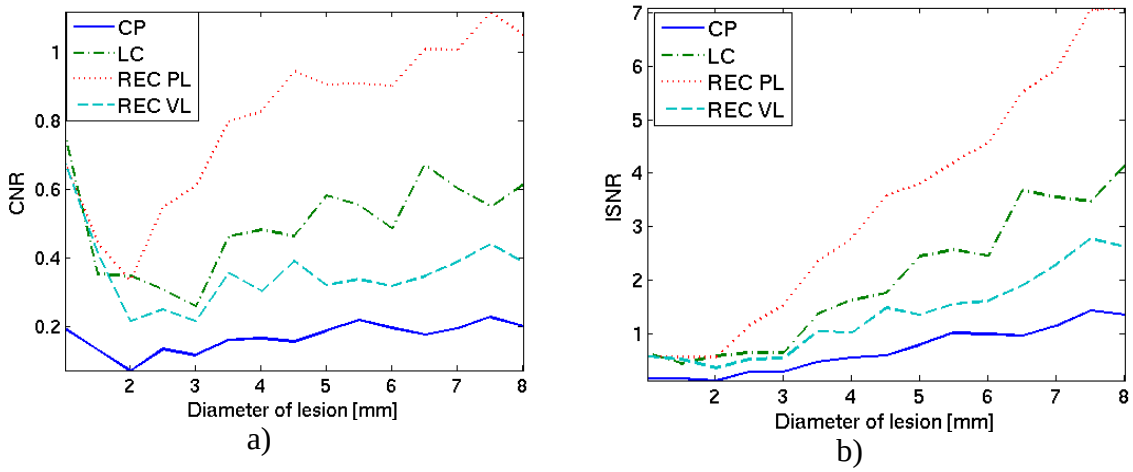

Figure 3.1. Simulation results for the -12 dB contrast lesions, (a) CNR of the -12 dB contrast lesions, (b) lSNR of the -12 dB contrast lesion.

The B-mode images corresponding to one trial of the 5-mm diameter lesion are displayed in Figure 3.2a-d. The CNR, lSNR, and eSNR for the 5-mm diameter lesion are also recorded in Table 3.1. Based on the metrics, however, REC PL achieved the highest CNR and lSNR, 1.22 and 5.13, respectively. The LC achieved the highest eSNR at 24.5 dB. In this case, REC VL actually outscored the LC with respect to lSNR at 4.70 compared to 4.47, respectively. However, this is not a trend as the aggregate LC outscored REC VL with respect to CNR and lSNR after averaging multiple trials (Figure 3.1a-b). Lastly, one of the 0.5-mm diameter lesions is shown in Figure 3.3. For all excitation types, no lesion is visually apparent. This corresponds to the limits of detection of the imaging system.

Table 3.1. 5-mm lesion metrics for the different excitation methods.

Excitation	**CNR**	**lSNR**	**eSNR (dB)**
CP	0.85	3.56	8.4
LC	1.06	4.47	24.5
REC PL	1.22	5.13	15.1
REC VL	1.12	4.70	13.0

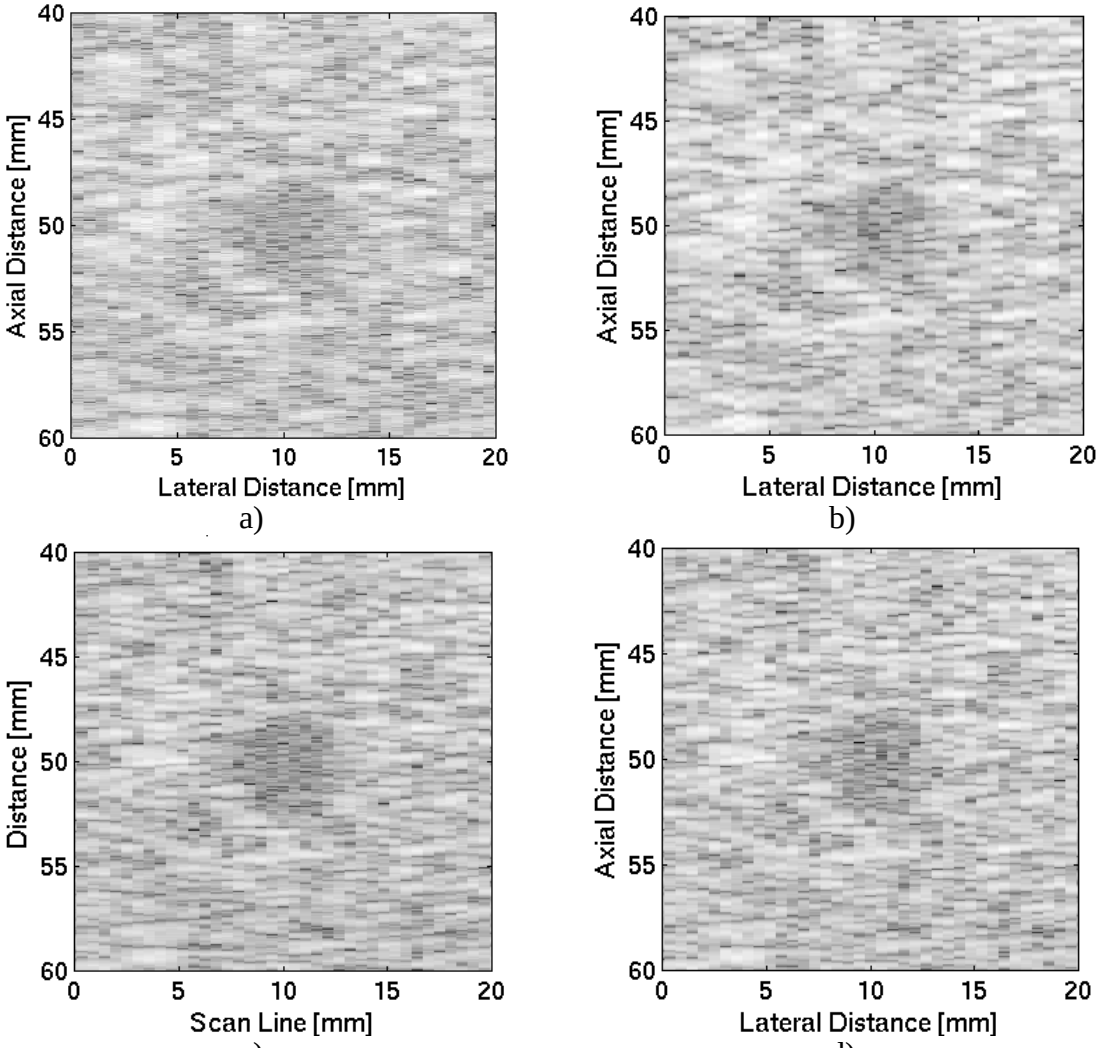

Figure 3.2. 5-mm lesion (a) CP, (b) LC, (c) REC PL, (d) REC VL.

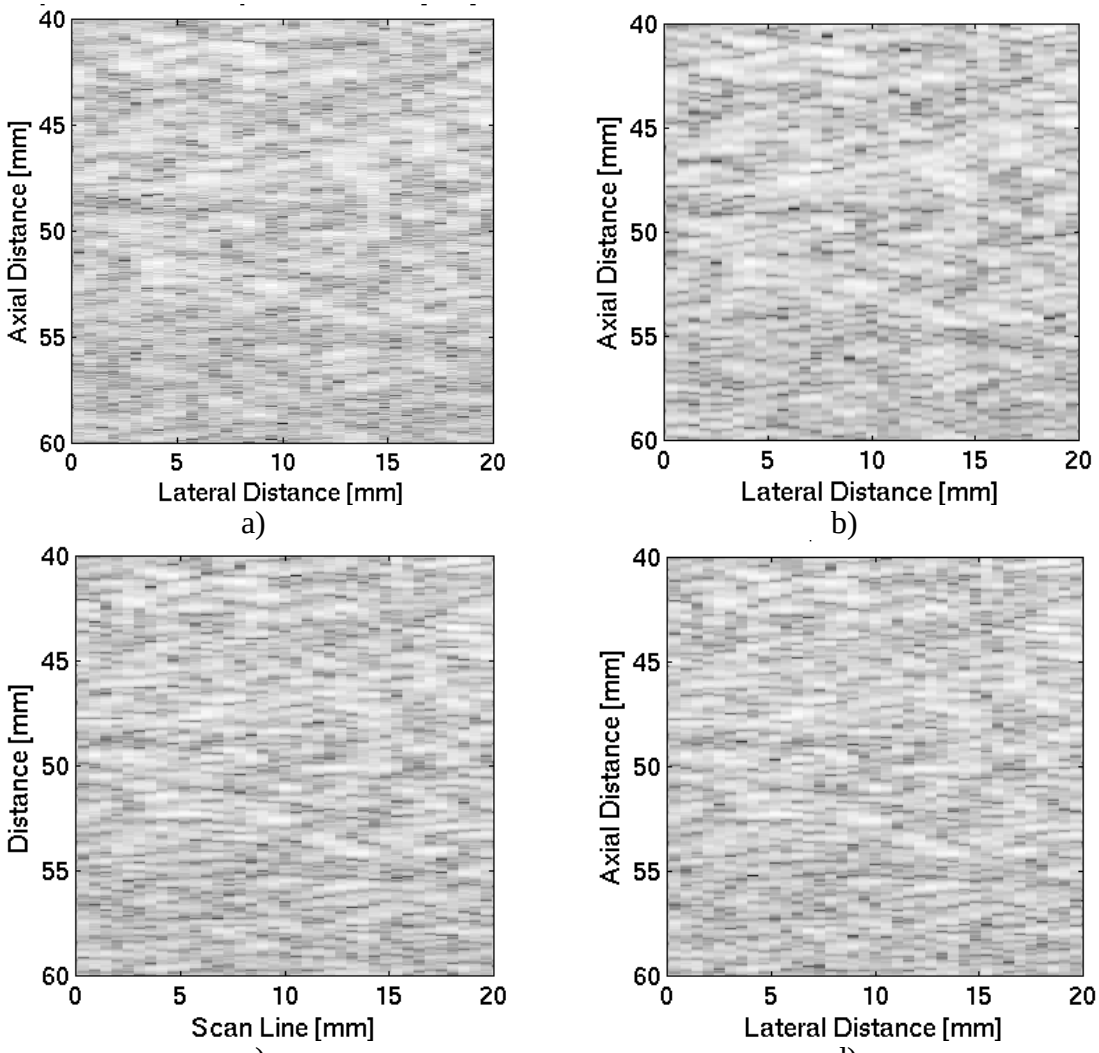

Figure 3.3. 0.5-mm lesion (a) CP, (b) LC, (c) REC PL, (d) REC VL.

Chapter 4 Results: Small Lesion Detectability

4.1 Description of Study

Small lesion detectability was mentioned in Chapter 1 as critical for clinical ultrasonic scanners. This study compared the ability of the REC technique to detect small lesions to that of other pulsing techniques such as the conventional pulse (CP) and the linear chirp (LC).

4.2 Results and Discussion

4.2.1 Simulations

To test the pulsing methods before use in Field II or in experimental data, a simple planar reflector was used to estimate the impulse response of the transducer. The excitation waveforms were convolved with the impulse response of the transducer and then Gaussian white noise was added. The two coded waveforms (LC and REC) were then compressed with their respective filters. This simulated a planar reflector but also assumed that the propagation was linear and also assumed no frequency dependent attenuation. The simulated transducer center frequency was 2.25 MHz with fractional bandwidth of 48%. The desired impulse response center frequency was 2.25 MHz with a fractional bandwidth of 96%, effectively doubling the transducer bandwidth. The time-bandwidth product was calculated by taking the -3-dB bandwidth of the coded chirp and multiplying it by the duration of the chirp. The LC's TBP was the product of the waveform duration, 26.3 μs, and the -3-dB bandwidth of chirp, 1.39 MHz, yielding a product of 36.6. Thus the expected improvement in eSNR between pre-compression and post-compression was about 15.6 dB. The pre-enhanced chip was 26.2 μs in duration and

the -3-dB bandwidth of the desired impulse response was 3 MHz which corresponded to a TBP of 78.6. Thus the expected gain in eSNR was 20 dB. To validate this the CP was simulated and noise added to achieve an eSNR of 23.9 dB. The same noise component was added to LC and REC simulations. The pre-compression eSNR values of the two coded waveforms were 24.8 dB and 24.5 dB for the LC and the REC waveform, respectively. The post-compression eSNR values were 42 dB for both techniques which corresponded to a gain of 17.2 dB and 17.5 dB for the LC and the REC technique, respectively.

Then the excitation methods were tested using Filed II and the simulated phantoms described in Section 2.5.1 The gain in eSNR for the two coded methods, LC and REC, were approximately equal, 14.6 and 14.3 dB, respectively. Table 4.1 lists the eSNR estimates after compression with respect to the three excitation methods. The CP required no post processing and therefore 0 dB gain is reported. The gain achieved for both the LC and the REC technique were dependent on the compression filters. The gain was calculated by comparing the eSNR of the pre-compressed to the compressed B-mode image. The values reported are averages over the 150 simulations.

The estimates of the resolution cell volume based on the speckle analysis are listed in Table 4.2. The REC technique outperformed the other two techniques in the lateral and axial directions. The axial estimate for the REC technique was 0.25 mm compared to 0.33 mm and 0.40 mm for the CP and the LC, respectively. In the lateral dimension, REC achieved 0.78 mm compared to 0.88 mm and 0.97 mm for CP and the LC, respectively. The resolution cell volume and eSNR estimates, Table 4.1 and Table

4.2, have only been reported for the -12-dB simulation. As these metrics are independent of lesion size, similar results were expected for different lesion contrasts.

Table 4.1. The eSNR is estimated based on the variance of the speckle at the focus (signal) and the variance of the simulated water bath (noise). The above results are an average of 150 simulations.

Excitation	eSNR (dB)(Avg.)	Gain (dB)(Avg.)
CP	17.2	0.0
LC	31.8	14.6
REC	30.5	14.3

Table 4.2. S_{cx} and S_{cz} estimate of 150 simulated phantoms.

Excitation	S_{cz} (mm)(Avg.)	S_{cx} (mm)(Avg.)
CP	0.33 ± 0.03	0.88 ± 0.09
LC	0.40 ± 0.04	0.97 ± 0.10
REC	0.25 ± 0.02	0.78 ± 0.08

Figure 4.1a-d shows the results for the two sets of simulations. Figure 4.1a and b are plots of the CNR and lSNR scores for 150 lesions with a simulated +6 dB lesion-to-background contrast. Figure 4.1c and d are the results of the 150 phantoms with -12 dB lesion-to-background contrast. The +6 dB simulation indicated no best method for increasing the CNR (Figure 4.1a). However, the gains in spatial resolution using REC resulted in higher lSNR values compared to CP and the LC for all lesion sizes (Figure 4.1b). The numerator of the lSNR function includes an estimate of the CNR and the diameter of the lesion. The denominator contains an estimate of the resolution cell volume. Thus, it was expected for the lSNR to tend toward zero as the lesion became smaller. The results of the CNR from the simulated lesions of -12 dB contrast are given in Figure 4.1c. The CNR values obtained using the REC technique were higher than the

CNR values estimated for CP and LC for all lesions greater than 2-mm in diameter. However, observation of the curves in Figure 4.1a suggests that the behavior of the CNR estimate may become more erratic at smaller lesion sizes. In all cases, the lSNR was higher for the REC technique compared to the other techniques (Figure 4.1b). B-mode images of the 5-mm lesion for the three excitation types and contrast types are shown in Figure 4.2 and Figure 4.3. The B-mode images indicate that the REC technique improved spatial resolution by the smaller speckle size apparent in the axial direction.

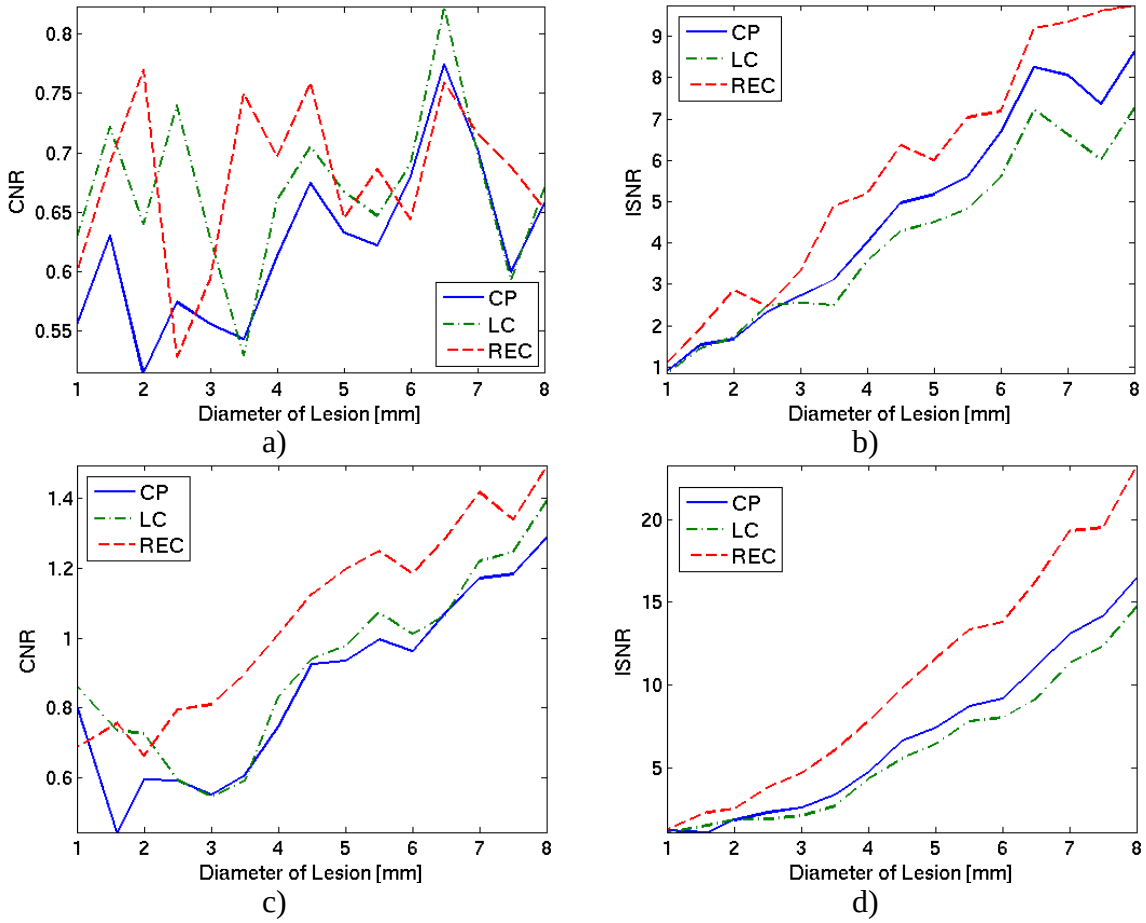

Figure 4.1. Simulation results for the +6 dB and -12 dB contrast lesions, (a) CNR of the +6 dB contrast lesions, (b) lSNR of the +6 contrast lesion, (c) CNR of the -12 dB contrast lesion, and (d) lSNR of the -12 dB contrast lesion.

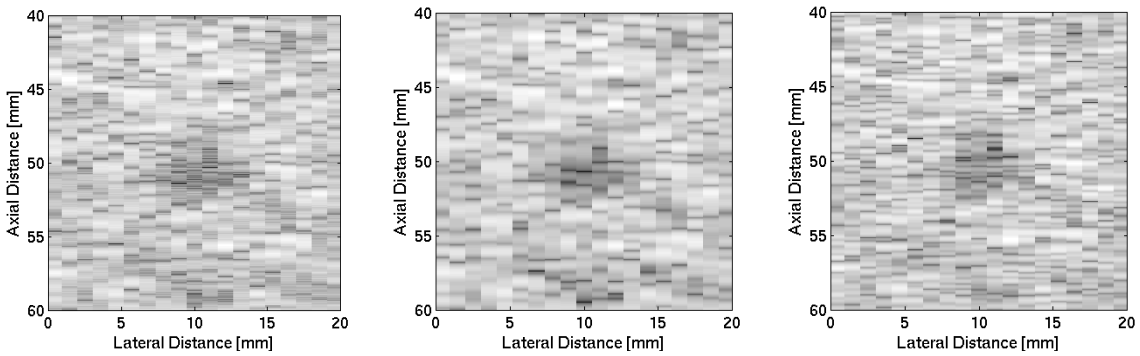

a) b) c)

Figure 4.2. 5-mm lesion with -12 dB contrast (a) CP, (b) LC, and (c) REC.

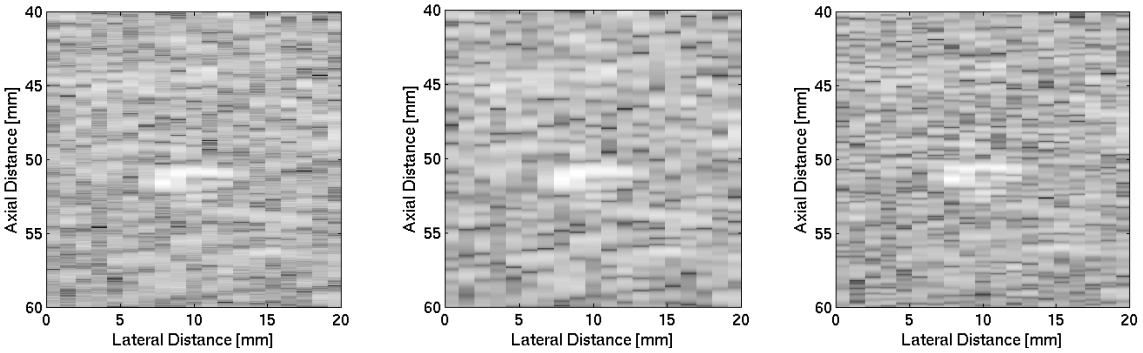

a) b) c)

Figure 4.3. 5-mm lesion with +6 dB contrast (a) CP, (b) LC, and (c) REC.

The erratic CNR curves for the smaller lesions suggested that the number of image samples available for the CNR calculation for small lesions may be too low to achieve good accuracy and precision compared to larger lesions. The CNR quality metric includes the variance of the area inside and outside the inclusion. As the inclusion becomes smaller and smaller there are also fewer data points to make an accurate estimate of the variance of the target region. It is presumed that a certain number of samples are needed before an accurate estimate can be obtained. The bias and variance of the CNR estimate may also be a function of the resolution cell volume. For a given region of interest size used to calculate CNR, a better spatial resolution should lead to an improved CNR estimate.

The dependence of the CNR calculation on the region of interest size and the spatial resolution were examined using simulations. Ten simulated phantoms were generated with 15 scatterers per resolution cell placed spatially at random. A simulated lesion of 8-mm diameter was positioned at the center of the phantoms with mean scatterer strength of -12 dB with respect to the background scatterer strength. Using Field II an f/3 transducer was translated laterally with half a beamwidth overlap to generate RF data. Field II also allows the impulse response of the transducer to be set. In this simulation the pulse/echo impulse response was a sinusoid centered at 2.25 MHz and windowed with a Blackman window. The -3 dB pulse-echo fractional bandwidth of the transducer was 48%.

To test the dependence of CNR on pulse length, excitation of a pulse (CP), single cycle, two cycle, and four cycle sinusoid centered at 2.25 MHz were tested. RF data of the ten phantoms imaged with these four excitation schemes were generated. The CNR was then calculated in regions ranging from approximately 6% to 100% of the size of the lesion which corresponded to 24 – 7,500 data points, respectively. From Figure 4.4b, the number of data points needed before an estimate with a bias less than 0.1 could be acquired was greater than 3,000 for CP. Therefore, if the size of the lesion is too small relative to the spatial resolution of the imaging system, the accuracy and precision of the CNR and lSNR estimates degrade. Furthermore, the results suggest that fewer samples are needed for CNR calculations for shorter duration pulses. Fewer samples are needed to get a good estimate of CNR with shorter pulses, i.e., larger bandwidth, because for samples coming from a region of specified size, shorter pulses result in more independent

samples in the region. Improving the axial resolution of an imaging system should lead to better CNR estimates for smaller samples sizes.

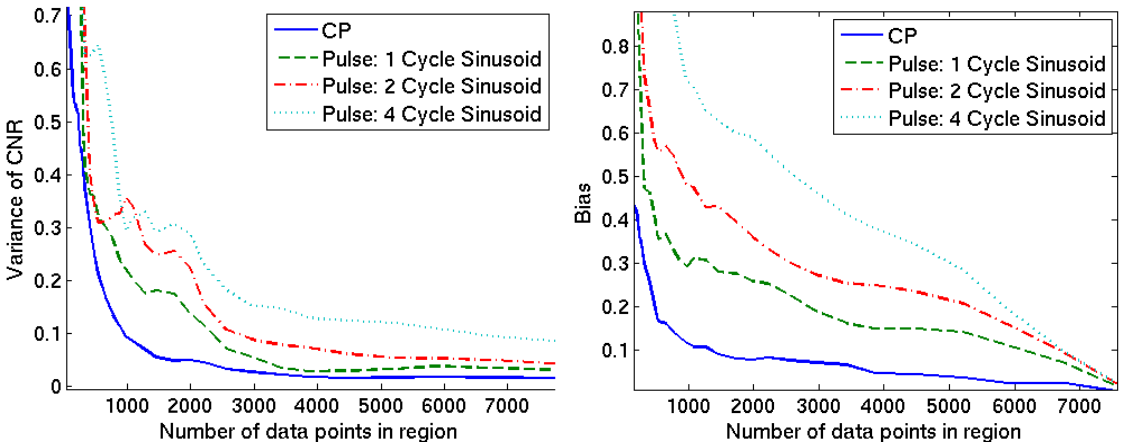

Figure 4.4. Results of 10 simulated phantoms, (a) variance of CNR versus number of data points used to calculate variance of region, (b) bias estimate for Field II simulations.

4.2.2 Experimental

The theoretical resolution from the transducer properties and estimated resolution cell size from the speckle analysis are reported in Table 4.3. A gain in lateral and axial resolution was achieved using REC. The axial resolution of REC (0.21 mm) outperformed the other two techniques (0.28 mm) of CP and the LC. Unexpectedly, the lateral resolution estimate for REC (1.35 mm) also improved over the other two methods (1.7 mm). The eSNR values and the gain in eSNR from compression for all techniques are listed in Table 4.4. The TBP of the excitation waveform was 40, so the expected gain in eSNR would be approximately 16 dB. However, this gain is the best estimate for the matched filtering case. The LC compression filter was tuned closer to a matched filter than the REC technique which produced a higher eSNR gain at the expense of axial

resolution (10.66 dB average gain and 0.28 mm axial resolution with LC versus 5.74 dB gain and 0.21 mm axial resolution with REC).

Table 4.3. Lateral and axial speckle cell volume estimate of experimental phantom.

	S'_{cx} (mm)	S'_{cz} (mm)	S_{cx} (mm)	S_{cz} (mm)
CP	1.6	0.80	1.70	0.28
LC	1.6	0.80	1.70	0.28
REC	1.6	0.40	1.35	0.21

Table 4.4. Experimental results for eSNR (dB) and the gain (dB).

Diameter	**3 mm**		**5 mm**		**8 mm**		**Avg.**	**Avg.**
Excitation	eSNR	Gain	eSNR	Gain	eSNR	Gain	eSNR	Gain
CP	9.08	0	9.35	0	9.43	0	9.29	0
LC	19.92	10.9	21.53	11.0	19.61	10.2	20.4	10.7
REC	15.08	6.0	14.80	4.2	16.42	6.7	15.4	5.7

The experimental data consisted of three slices perpendicular to the main axis of the cone phantom. The phantom was scanned at slices corresponding to a cone diameter of 3, 5, and 8 mm. The noise power was estimated by taking the variance of the signal corresponding to the water bath before the phantom. The signal power from the scatterers was estimated by taking the variance of a line of speckle along the axial direction at the depth of the lesion (68 cm).

The 5-mm B-mode image of the three excitations types is displayed in Figure 4.5. The number of data points used for calculation of CNR and lSNR for the 3-mm lesion was 3,262 points. As found previously, the lack of sample points may result in less reliable estimates of CNR. The number of points used in the 5-mm and 8-mm lesion was 9,123 and 23,429, respectively. The CNR and lSNR values for all cases are listed in Table 4.5.

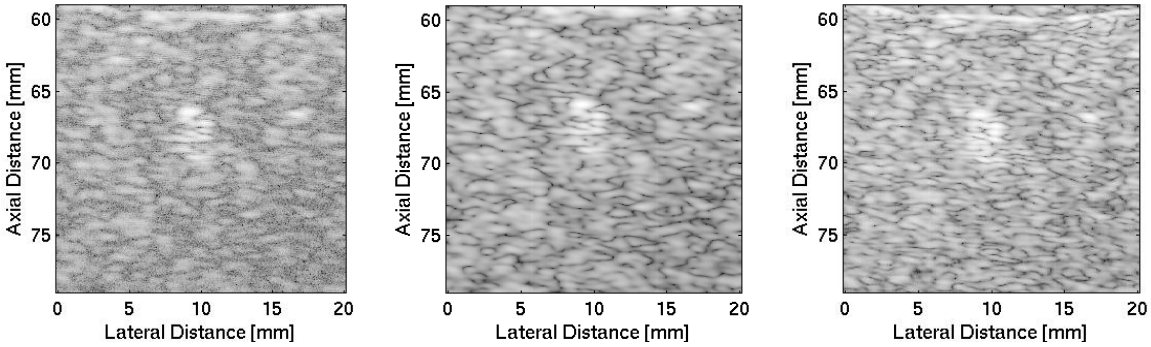

a) b) c)

Figure 4.5. The 5-mm slice: (a) CP, (b) LC, and (c) REC.

Table 4.5. Experimental results for CNR and lSNR.

Diameter	**3 mm**		**5 mm**		**8 mm**	
Excitation	CNR	lSNR	CNR	lSNR	CNR	lSNR
CP	1.41	6.14	1.06	7.67	0.80	9.22
LC	1.32	5.80	1.13	8.30	0.93	10.34
REC	1.26	7.08	1.29	12.05	0.97	14.50

The CNR for REC outperformed the LC and CP in the detectability of the 5-mm and 8-mm lesions. The poor performance in the 3-mm case with respect to REC and CNR could be attributed to a lack of sufficient data points. In addition, small sample size could also be an issue (one cone phantom). However, the lSNR metric was higher for REC even though the CNR score was lower in the 3-mm case. This can be attributed to the significant increase in axial resolution achieved with the REC technique. The increase in axial resolution dominated the REC lSNR score. The lSNR score was boosted by 15%, 45%, and 40% for the 3, 5, and 8-mm lesions respectively.

Chapter 5 Conclusions

The ability of an ultrasonic imaging system to detect focal lesions against a background is of paramount importance. Of special interest is the detection of small, low contrast targets because this is one of the practical limitations of an ultrasonic imaging system. ROC curves take months to generate and require clinicians, ground truth, and histology to formulate. Contrast/detail analysis is a way to quickly evaluate an imaging system's performance of small, low contrast targets. The lSNR is a metric that combines CNR, resolution cell size, and the diameter of a lesion to provide information for lesion detectability of an imaging system. The lSNR metric allows the primary evaluation of an imaging system or modification to an imaging system, without the effort involved in providing ROC curves.

The first study on the limitations of REC showed that if the system is pressure limited at the focus, REC will achieve the highest lSNR (lesion detectability). However, if the system is voltage limited, then the REC technique did not quite match the linear chirp though it did outperform conventional pulsing. In the future a similar study should be performed experimentally to validate simulations.

In the second study, the REC technique improved lesion detectibility for all of the simulated and experimental cases. In experiments the lSNR was increased by 16%, 56%, and 32% for the 3, 5, and 8 mm lesions, respectively. The low estimate of CNR for the 3 mm diameter phantom in the experimental case may be due to a poor estimate because of a low number of samples available. Even so, the boost in bandwidth by the REC technique improved lSNR for the 3-mm case. Therefore, according to the lSNR metric

the REC technique improved the performance of the ultrasonic imaging system to detect small lesions. This may have significance for medical diagnostics. However, only a fixed focus system has been considered. Of interest is the effect of REC on a dynamic focus system which may be explored in future studies.

The REC technique also improved eSNR while boosting the axial resolution over the conventional pulsing technique. The REC technique boosted energy in transition bands of the transducer which in turn increased the usable bandwidth of the transducer. The increase in the usable bandwidth resulted in an improved axial resolution. That is, at the same eSNR the REC filter should be able to operate closer to an inverse filter, improving axial resolution.

References

[1] Szabo T. *Diagnostic Ultrasound: Inside Out*, Burlington: Elsevier Inc, 2004.

[2] Khuri-Yakub, B.T., Oralkan, O., and Kupnik, M. "Next-gen ultrasound," *IEEE Spectrum*, vol. 46. no. 5, pp. 45-52, May 2009.

[3] Wild, J.J., and Reid, J.M., "Application of echo-ranging techniques to the determination of structure of biological tissues," *Science*, vol. 115, pp. 226-230, 1952.

[4] Lizzi, F., Greenebaum E., and Feleppa E., "Theoretical framework for spectrum analysis in ultrasonic characterization", *Journal of the Acoustical Society of America*, vol. 73, no. 4, pp. 1366-1373, Apr. 1983.

[5] Smith, S., and Lopez, H., "A contrast-detail analysis of diagnostic ultrasound imaging," *Medical Physics*, vol. 9, no. 1, pp. 4-12, Jan./Feb. 1982.

[6] Smith, S.W., Wagner, R.F., Sandrik, J.M., and Lopez, H., "Low contrast detectability and contrast/detail analysis in medical ultrasound," *IEEE Transactions on Sonics and Ultrasonics,"* vol. 30, no. 3, pp. 164-173, May 1983.

[7] Bamber, J.C., Speckle reduction, Chapter 5, pp. 55-67, in: *Advances in Ultrasound Techniques and Instrumentation (Clinics in Diagnostic Ultrasound*, vol. 28, P.N.T. Wells (Ed.), New York: Churchill Livingstone, 1993, pp. 55-67.

[8] Cobbold R.S.C., *Foundations of Biomedical Ultrasound*, New York: Oxford University Press, 2007.

[9] O'Brien, W.D., "Assessing the Risks for Modern Diagnostic Ultrasound Imaging," *Japanese Journal of Applied Physics*, vol. 37, pp. 2781-2788, May 1998.

[10] Chiao, R.Y., Hao, Xiaohui, H., "Coded excitation for diagnostic ultrasound: a system developer's perspective," *IEEE Transactions on Ultrasonic, Ferroelectrics, and Frequency Control*, vol. 52, no. 2, pp.160-170, Feb. 2005.

[11] Wagner, R.F., Smith, S.W., Sandrik, J.M., and Lopez, H., "Statistics of speckle in ultrasound B-scans," *IEEE Transactions on Sonics and Ultrasonics*, vol. 30, no. 3, pp. 156-163, May 1983.

[12] Dahl, J.J., Guenther, D.A., and Trahey, G. "Adaptive imaging spatial compounding in the presence of aberration," *Transactions on Ultrasonics, Ferroelectrics, and Frequency Control*, vol. 52, no. 7, pp. 1131-1144, July 2005.

[13] Nathanson F.E., *Radar Design Principles*, 2d ed. New York: McGraw-Hill, 1991.

[14] Skolnik M.I., *Introduction to radar systems*, New York: McGraw-Hill, 1962.

[15] Takeuchi, Y. "An investigation of a spread energy method for medical ultrasound systems part one: theory and investigation," *Ultrasonics*, vol. 17, pp. 175-182, July 1979.

[16] Misaridis, T., and Jensen, J.A., "Use of modulated excitation signals in medical ultrasound. part II: design and performance for medical imaging applications," *IEEE Transactions on Ultrasonics, Ferroelectrics, and Frequency Control* vol. *52*, no. 2, pp. 192-206, Feb. 2005.

[17] Misaridis, T., and Jensen, J.A., "Use of modulated excitation signals in medical ultrasound. part I: basic concepts and expected benefits," *Transactions on Ultrasonics, Ferroelectrics, and Frequency Control,* vol. *52*, no. 2, pp. 177-191, Feb. 2005.

[18] North, D.O., "An analysis of the factors which determine signal/noise discrimination in pulsed-carrier systems," *Proceeding of the IEEE*, vol. 51, no. 7, pp. 1016-1027, July 1963.

[19] Proakis, J.G., and Salehi, *Communications systems engineering*, 2d ed., New Jersey: Prentice-Hall, 2002.

[20] Haider, B., Lewin, P.A., and Thomenius, K.E., "Pulse elongation and deconvolution filtering for medical ultrasonic imaging," *Transactions on Ultrasonics, Ferroelectrics, and Frequency Control,"* vol. 45, no. 1, pp. 98-112, Jan. 1998.

[21] Oelze, M.L., "Bandwidth and resolution enhancement through pulse compression," *Transactions on Ultrasonics, Ferroelectrics, and Frequency Control*, vol. 54, no. 4, pp. 768-781, April 2007.

[22] Sanchez, J., and Oelze, M.L., "An ultrasonic imaging speckle-suppression and contrast enhancement technique by means of frequency compounding and coded excitation," *Transactions on Ultrasonics, Ferroelectrics, and Frequency Control*, vol. 56, no. 7, pp. 1327-1339, July 2009.

[23] Sanchez, J, and Oelze, M.L. "A novel coded excitation scheme to improve spatial and contrast resolution of quantitative ultrasound imaging," *Transactions on Ultrasonics, Ferroelectrics, and Frequency Control,* vol. 56, no. 10, pp. 2111-2123, Oct. 2009.

[24] Pollakowski, M., Ermert, H., Bernus L.V., Schmeidl, S., "The optimum bandwidth of chirp signals in ultrasonic applications," *Ultrasonics*, vol. 31, no. 6, pp. 417-420, 1993.

[25] Lei., L., Heng, Z., Shankai, G., "Barker cod in TCD ultrasound systems to improve the sensitivity of emboli detection," *Ultrasound in Medicine & Biology*,

vol. 35, no. 1, pp. 94-101, 2009.

[26] Golay, M.J.E., "Complementary Series," IRE Transaction on Information Theory, vol. IT-7, pp. 82-87, April 1961.

[27] Takeuchi, Y. "An investigation of a spread energy method for medical ultrasound systems part two: proposed system and possible problems," *Ultrasonics*, vol. 17, pp. 219-224, Sept. 1979.

[28] Tsou, J.K., Liu, J., and Insana, M.F., "Modeling and phantom studies of ultrasonic wall shear rate measurements using coded excitation," *Transactions on Ultrasonics, Ferroelectrics, and Frequency Control,* vol. 53, no. 4, pp. 724-734, April 2006.

[29] Beutel, J., Kundel, H.L., and Van Metter, R.L., *Handbook of medical imaging,* Bellingham, WA: SPIE Press, 2000.

[30] Jensen, J.A., "Field: A Program for Simulating Ultrasound Systems," *Tenth Nordic-Baltic Conference on Biomedical Imaging Published in Medical & Biological Engineering & Computing*, pp. 351-353, vol. 34, Supplement 1, Part 1, 1996.

[31] Jensen, J.A., and Svendsen, N.B., "Calculation of pressure fields from arbitrarily shaped, apodized, and excited ultrasound transducers," *Transactions on Ultrasonics, Ferroelectrics, and Frequency Control,* vol. 39, no. 2, pp. 262-267, March 1992.

[32] Sanchez, Jose. Improving Ultrasonic Imaging using novel coded excitation, Ph.D. dissertation, Dept. of Electrical and Computer Engineering, University of Illinois, Urbana, IL, USA, 2010.